Sparse haplotype-based fine-scale local ancestry inference at scale reveals recent selection on immune responses

Yaoling Yang[1,2,✉], Richard Durbin[3], Astrid K. N. Iversen[4], and Daniel J. Lawson[1,2,✉]

[1]Department of Statistical Sciences, School of Mathematics, University of Bristol, Bristol, UK

[2]MRC Integrative Epidemiology Unit, Population Health Sciences, University of Bristol, Bristol, UK

[3]Department of Genetics, University of Cambridge, Cambridge, UK

[4]Nuffield Department of Clinical Neurosciences, John Radcliffe Hospital, University of Oxford, Oxford, UK

✉Corresponding authors: Yaoling Yang (yaoling.yang@bristol.ac.uk) and Daniel J. Lawson (dan.lawson@bristol.ac.uk)

Abstract

Increasingly efficient methods for inferring the ancestral origin of genome regions are needed to gain new insights into genetic function and history as biobanks grow in scale. Here we describe two near-linear time algorithms to learn ancestry harnessing the strengths of a Positional Burrows-Wheeler Transform (PBWT). SparsePainter is a faster, sparse replacement of previous model-based 'chromosome painting' algorithms to identify recently shared haplotypes, whilst PBWTpaint uses further approximations to obtain lightning-fast estimation optimized for genome-wide relatedness estimation. The computational efficiency gains of these tools for fine-scale local ancestry inference offer the possibility to analyse large-scale genomic datasets in completely novel ways. Application to the UK Biobank shows that haplotypes better represent ancestries than principal components, whilst linkage-disequilibrium of ancestry identifies signals of recent changes to population-specific selection for many genomic regions associated with immune responses, suggesting new avenues for understanding the pathogen-immune system interplay on a historical timescale.

Introduction

Modern human populations are complex mixtures between ancient contributing source groups[1]. Genetic admixture is the process of mixing groups that were genetically distinct due to genetic drift, which can create new distinct populations[2,3]. The process is ubiquitous and spans scale in space and time, from the admixture with Neanderthals around 50,000 years ago when modern humans migrated out of Africa[4], to native Americans mixing with primarily European and African immigrants over the last 500 years to form the majority of United States ancestry[5], and the fine-scale geographical regionalisation within a single country such as the UK[6]. The identification of chromosomal regions originating from a specific population is known as local ancestry inference (LAI)[7], which can be used to map disease loci[8], investigate the relationships between modern populations, improve association studies[9], and study demographic histories[10].

Genome-wide association studies (GWAS) have identified single nucleotide polymorphisms (SNPs) associated with human complex traits and diseases[11], but the SNP frequencies are likely to be associated with particular ancestries. Local ancestry may then either be viewed as a confounder of the SNP effect[9], or treated as a predictor as in 'Ancestral GWAS'[12]. In this framing, local ancestry inference examines the ancestral origin of risk loci in terms of a population and a time — for instance, risk alleles associated with multiple sclerosis originated from pastoralists dwelling on the Pontic Steppe, which were brought into Europe by the Yamnaya-related migration around 5,000 years ago[12]. Other examples include the relationship between platelet count in Hispanics and an Amerindian-origin variant of the ACTN1 gene[13], a link between quantitative red blood cell traits and African- and Amerindian-origin loci in the HBA1/2 gene[14], and kidney disease in African-origin variants of the APOL1 gene[15].

It is hard to perform LAI accurately and efficiently. Various LAI software have been developed since the 21st century, and the majority[16] are based on the Li and Stephens hidden Markov model (HMM)[17], including HAPMIX[7], ChromoPainter[18], LAMP-LD[19], MOSAIC[3] and FLARE[20]. HAPMIX pioneered this application but is limited to modelling two ancestries. In comparison, ChromoPainter enables the accurate analysis of admixtures from multiple groups but is slow. LAMP-LD is faster but can be unstable[16]. The distinctive feature of MOSAIC is that the knowledge of the intricate connections between reference haplotypes and ancestral mixing groups is not required[3]. Recently, through the on-the-fly compression of reference panels, saved checkpoints and composite reference haplotypes, FLARE greatly improves the computational performance compared with the previous LAI software[20]. Other approaches for local ancestry inference are also possible, among which PCAdmix, a Principal Components-based algorithm[21], and RFMix[22], which employs a discriminative modelling strategy, are popularly used.

Our technical contribution is providing two algorithms that fulfil different use cases. Both are significantly faster than anything previously reported, especially for identifying fine-scale population structure. The most rapid is orders of magnitude faster, opening the application to hundreds of thousands or even millions of samples as presented by the most challenging modern biobanks and association studies. These approaches avoid storing the entire genotype information in memory, instead using the Positional Burrows-Wheeler Transform (PBWT)[23,24] to extract only a sparse set of the longest haplotype matches to the reference panel at each position. In PBWTpaint, only the longest *set-maximal* matches are retained, which we will show is sufficient for genome-wide ancestry. In SparsePainter, we extract a richer set of haplotypes on which we show that a sparse implementation of the Li and Stephens HMM model[17] can be run with a negligible accuracy cost by using a Hash Map data structure[25].

Having access to local ancestry information at scale presents novel opportunities for identifying genomic features that are of biological significance. Within SparsePainter we are able to efficiently compute Linkage Disequilibrium of Ancestry (LDA), LDA score (LDAS) and Ancestry Anomaly Score (AAS)[12] at scale, which are recently proposed summary statistics of local ancestry that are predicted under recent population-specific selection. LDA is the correlation of ancestries between SNP pairs, which measures whether recombination events between ancestries are more frequent than those within

ancestries. LDAS calculates the total LDA of each SNP on the chromosome weighted by genetic distance. A lower LDAS indicates the haplotype inherited from the reference population is shorter than expected. We identify two mechanisms that generate low LDAS and both involve a change in selection between the pre-existing and admixed population. The first involves selection on a nearby locus, leading to balancing selection at the level of haplotypes. The second is against a locus that was high frequency in at least one contributing population. AAS is the degree of difference between the estimated average ancestry probabilities and the genome-wide average, which detects signals of recent selection for loci experiencing changes in ancestry frequencies.

We benchmarked SparsePainter against ChromoPainter and FLARE, which demonstrates that SparsePainter is faster both empirically and in scaling, particularly at fine scale, i.e. as the number of reference populations grows. Even more astonishingly, PBWTpaint is faster than all methods by orders of magnitude in identifying genome-wide haplotype structure within a single dataset, which is its specific capability.

In exploring population structure within the UK Biobank (UKB) with PBWTpaint, we construct haplotype principal components (HCs) which we compare to the widely-used SNP-based principal components (PCs). HCs are better associated with birthplace and seem to capture more nuanced genetic variation than PCs, revealing distinct ancestral patterns among ethnic backgrounds and significant regional distinctions within the UK and Ireland, suggesting potential for more refined population stratification in genetic studies. Using 1000 Genomes Project (1000GP) Data[26] as reference, we can apply the LDAS and AAS statistics to identify genes that show signals of recent changes to population-specific selection. This approach, applied genome-wide, identifies a number of genes that are almost entirely immune-related, pointing to population-specific immune response as a central driver of selection acting on historical timescales.

Results

Method Overview

There are two main approaches to ancestry inference. The first is *unsupervised learning*, which addresses the goal of learning fine-scale population structure. Examples include clustering[18], unsupervised admixture models[27,1], or dimensionality reduction such as Principal Component Analysis (PCA) based on either genotype[28,29] or haplotype data[18]. Here, the data are not typically curated and we aim to form the largest dataset possible for the analysis. The second approach is *supervised* learning, in which target individuals are compared to carefully curated reference populations, and recently admixed individuals (which are the majority of individuals) are not directly used. The goal of supervised learning divides into *ancestry estimation* which can be used analogously to unsupervised genome-wide ancestry profiles[30], or *local ancestry estimation* in which the ancestry of particular sections of DNA is inferred.

These goals are met by two tools that facilitate a completely new scale of haplotype-based ancestry

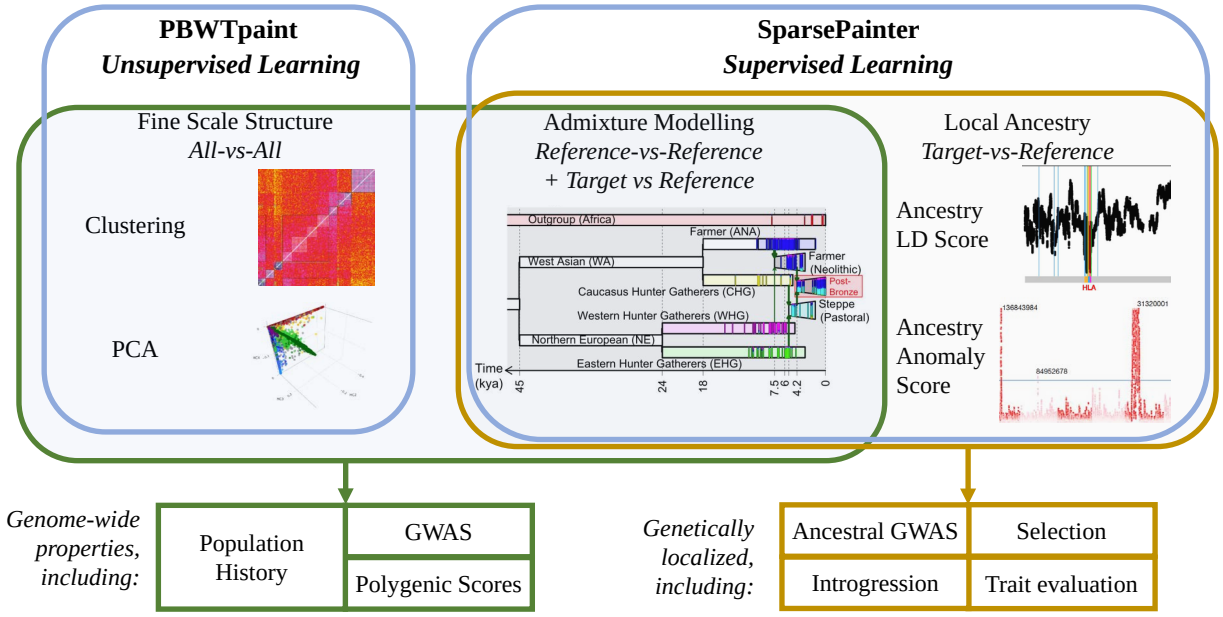

Fig. 1: **An overview of the functionalities of SparsePainter and PBWTpaint.** PBWTpaint performs *all-vs-all* painting, for use in fine-scale structure estimation via unsupervised learning approaches, such as clustering (plot from Lawson et al. (2012)[18] and PCA. Under supervised learning, SparsePainter performs *reference-vs-reference* painting for admixture estimation and *target-vs-reference* painting for local ancestry inference, such as LDAS and AAS (plots at right from Barrie et al. (2024)[12]).

analysis, as described in Fig. 1. The first of these is PBWTpaint, a direct extension of the PBWT[23] which rapidly identifies long matches. This uses two innovations to achieve extreme computational performance for unsupervised learning of a single dataset, comparing each individual to every other in *all-vs-all* painting. First, PBWTpaint only considers a very limited subset of possible matches representing the maximally shared haplotypes at any locus (called *set-maximal*). Further, the copying model, which via the HMM allows copying from any sample, is replaced with an approximation that only considers overlapping set-maximal matches. These approximations make for an approximately linear-time cost and mega-scale analyses are straightforward. Larger datasets uncover longer, more recent matches, and any inaccuracies due to modelling approximations average out over the whole genome for genome-wide analyses.

The second tool is SparsePainter, which is designed to perform accurate local ancestry inference efficiently. Whilst SparsePainter can perform *all-vs-all* painting, it is optimised for either painting a reference panel against itself (*reference-vs-reference* painting), or painting target individuals using a reference panel (*target-vs-reference* painting). Individuals from the reference and target datasets are *exchangeable* (see Methods): informally this makes downstream analysis unbiased by whether samples were in the reference. There are two primary outputs of SparsePainter. The first is local ancestry

estimates, which are the probabilities that a haplotype at a particular chromosomal location is inherited from each ancestral individual or population. The second is the expected fraction of the total genome shared most recently between a target and each reference ancestral individual or population. SparsePainter can efficiently compute the selection statistics LDA, LDAS and AAS.

PBWTpaint

Storing the genotype information of all the samples in memory is a problem for large datasets. The Positional Burrows-Wheeler Transform (PBWT)[23] is a data structure to transform a binary matrix X_{ik} (with $2N$ haplotypes and K SNPs) into a sequence of run-length compressed arrays per SNP, in each of which the haplotype values at the SNP are sorted according to the reversed haplotype prefixes preceding the SNP. From a PBWT, long matches can be efficiently extracted using the *ReportMatches* algorithm, and set-maximal matches with the *ReportSetMaximalMatches* algorithm, in $O(NK)$ operations for all haplotypes at the same time. Our models are built on these matches.

For each target individual i, PBWTpaint iterates through the $M(k)$ matches at a locus k (which are typically very sparse, and sparse by construction for set-maximal matches). For each matched reference haplotype j we extract the start s_{jk} and end e_{jk} positions of the maximal exact match to j covering k, i.e. s_{jk} is the location just after the first upstream mismatch, and e_{jk} is the location just before the first downstream mismatch. From these, we compute a weight $w_{jk} = (k - s_{jk})(e_{jk} - k)$, i.e. the weight increases linearly with distance from each end of the match, and quadratically with the total length of the match for positions at the midpoint of the match. This is normalised over matches j to give a local ancestry probability $p_{jk} = w_{jk} / \sum_{l=1}^{2N} w_{lk}$, which is summed over loci k to produce a genome-wide ancestry estimate p_j. We also provide estimates of the total number of recombination events, as well as regional bootstraps, to enable clustering with FineSTRUCTURE[18].

From PBWT to an accurate Sparse Data Matrix

For local ancestry inference, the longest haplotype matches at the target locus are the most important, since short matches appear within any ancestry due to statistical noise and incomplete lineage sorting, i.e. ancient structure shared across ancestries rather than recent genealogical relationships. As such, short matches provide little useful information for tracing local ancestry.

Whilst the original PBWT algorithm finds long matches only within the same database, it has been extended to report long matches between different haplotype sets[24]. For accurate and efficient local ancestry inference we detect all matches longer than some threshold L, but there may be no genome-wide 'correct' L. Some target haplotypes will only have short matches if they diverged a long time ago, and few or even no matches are longer than L. Other target haplotypes will share extremely long segments of DNA with many reference haplotypes leading to many matches being retained, the shorter of which (also longer than L) are not helpful for inferring ancestry. To address this barrier, we revisited the 'long match query' algorithm of PBWT and proposed the Algorithm 'ReportLongestMatches' which aims to find at least Q longest matches at each position for a target sample i (Methods). With this algorithm,

we maintain a particular sparsity level at each location while also preserving the longest matches to guarantee accuracy.

Using Hash Map to perform HMM Forward-Backward Algorithm in sparse form

SparsePainter stores haplotype matches in a Hash Map data structure that implements an associative array abstract data type for efficient key-value storage and retrieval[25], facilitating $O(1)$ storage and lookup of values (here painting probabilities) based on unique identifiers or keys (here haplotype indices). We then employ a sparse approximation to Li and Stephen's hidden Markov model (HMM) by vectorising the forward and backward probabilities and assuming a vanishing mutation rate (Methods). The forward and backward computation is only required within the Q longest matches to the target haplotype at each locus, allowing efficient computation of the local ancestry probabilities and the expected genome shared. Compared with computing and storing the probabilities at all N haplotypes, our approach reduces both memory usage and compute time from $O(N)$ to $O(Q)$.

Simulation overview

We used SLiM 3.7.1[31] to simulate genetic data on 100 megabases throughout 3000 generations, aiming to compare the accuracy, speed and memory utilization of SparsePainter, ChromoPainter, FLARE and PBWTpaint in terms of local ancestry and genome-wide estimates. These comparisons are sufficient because Browning et al. (2023)[20] demonstrated through simulation that for the specific task of supervised local ancestry inference FLARE matches MOSAIC in terms of accuracy and surpasses it in computational efficiency, and outperforms RFMix both in speed and accuracy. In our study, we used four distinct simulation models (see Methods for details):

- **Simulation 1**: A hierarchical model designed to assess the speed, memory usage, and accuracy of PBWTpaint, SparsePainter, and ChromoPainter for within reference (supervised or unsupervised) painting;
- **Simulation 2a**: An evolutionary process that generates from 2 to 100 different local ancestries, to investigate the scaling of SparsePainter and ChromoPainter in *target-vs-reference* painting;
- **Simulation 2b**: A less-separated version of Simulation 2 with limited populations, to assess the accuracy of *target-vs-reference* painting for SparsePainter, ChromoPainter, and FLARE;
- **Simulation 2c**: A larger-scale version of Simulation 2b to investigate how SparsePainter balances accuracy against speed and memory utilization in *target-vs-reference* painting.

Within-sample performance comparison

We first compared the efficiency of PBWTpaint (using *all-vs-all* painting) and SparsePainter and ChromoPainter (using *reference-vs-reference* painting) under Simulation 1. FLARE is excluded as it can neither perform within-sample, nor genome-wide, comparisons. Performance is measured using the *recovery rate* of an individual's own population ancestry fraction using squared Pearson's correlation coefficient (denoted as r^2) with the truth (Methods).

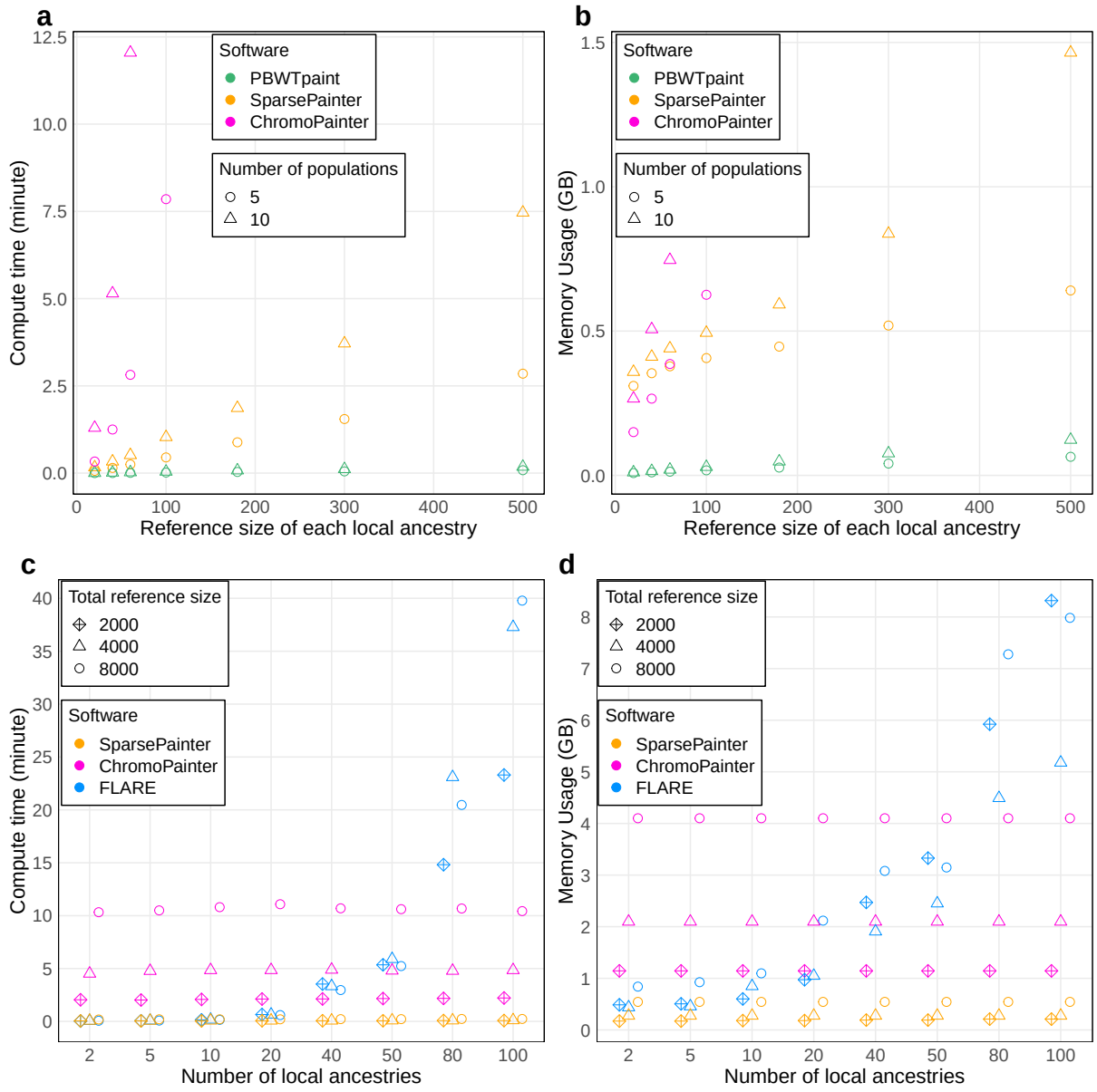

Fig. 2: **Speed and memory comparison between software.** a-b, Speed and memory of admixture estimates for *reference-vs-reference* painting between software with 5 or 10 local ancestries and different reference sizes with 5000 SNPs (Simulation 1). c-d, Speed and memory of painting 100 target individuals between software with different numbers of local ancestries and reference sizes with 2100 SNPs (Simulation 2a).

Fig. 2a-b illustrates that both in theory and practice, ChromoPainter has a quadratic cost as a function of panel size, so scales poorly to larger reference sizes. SparsePainter is close to linear in both speed and memory efficiency regardless of reference sizes. Whilst PBWTpaint also scales linearly, it is orders of magnitude faster, and only introduces a minor trade-off in terms of accuracy (Fig. 3a). Notably, PBWTpaint only retains accuracy for genome-wide estimation, as its simple model with set-

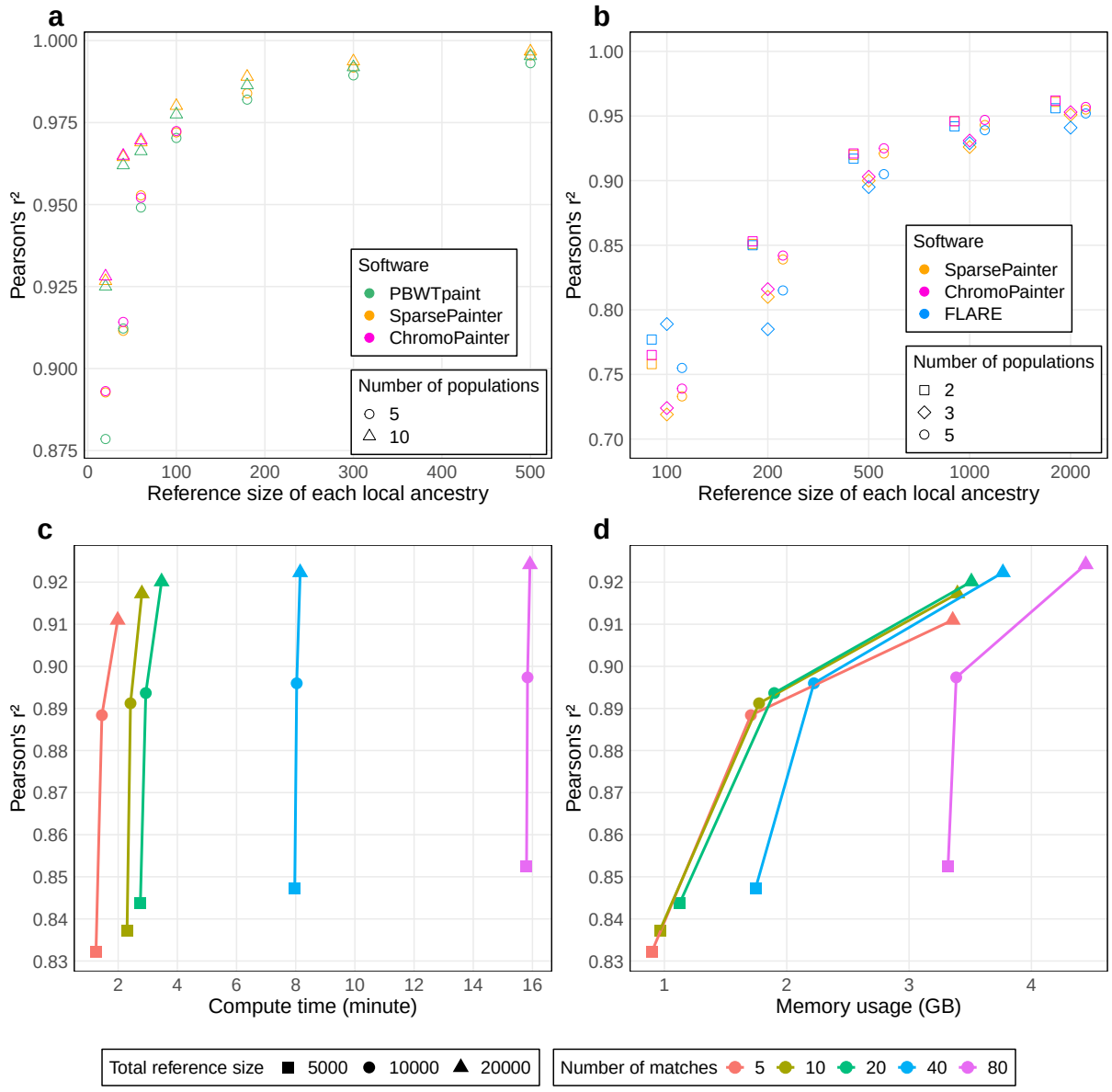

Fig. 3: **Accuracy of software and the trade-off between accuracy and computational cost in SparsePainter.** a, Self-recovery rate for *reference-vs-reference* painting with 5000 SNPs (Simulation 1). b, Accuracy of local ancestry estimates with 3600 SNPs and 50 target individuals sampled 13 generations after admixture (Simulation 2b). c-d: compute time and memory usage of SparsePainter for painting with different sparsity and reference sizes under a 5-way admixture model (Simulation 2c).

maximal matches isn't suitable for estimating local ancestries (Methods).

Target-vs-reference speed and memory comparison for LAI

As PBWTpaint neither can paint target samples against different reference panels, nor perform local

ancestry estimates, we restricted our speed and memory comparison to SparsePainter, ChromoPainter and FLARE with Simulation 2a. As all those software are based on the Li and Stephen's hidden Markov model, their computational costs for genome-wide and local ancestry estimates are expected to be similar.

The speed and memory of SparsePainter and ChromoPainter remain largely unaffected by the number of true local ancestries. Conversely, whilst FLARE demonstrates impressive speed and efficient memory usage with few local ancestries ($n_{pop} \leq 5$), its efficiency dramatically diminishes compared to SparsePainter when handling 20 or more local ancestries (Fig. 2c-d and Extended Data Fig. 2). Impressively, when painting with 100 local ancestries, SparsePainter is at least 100 times faster and 10 times more memory-efficient than FLARE.

A recent study[30] decomposed the UK Biobank into 129 distinct fine-scale reference ancestries. We replicated their analysis with the 4334 reference individuals from non-restricted data sources (i.e. all except POPRES) spanning 129 populations. For 1000 target individuals on chromosome 21 which comprises 9522 SNPs, SparsePainter is dramatically faster and requires minimal memory (6 minutes and 1.5GB) compared with ChromoPainter (272 minutes and 10.2GB) and FLARE (338 minutes and 14.2GB).

Target-vs-reference accuracy comparison for LAI and admixture estimation

While SparsePainter has demonstrated superior speed and memory than FLARE and ChromoPainter, it is crucial to maintain accuracy. In Simulation 2b we examined the accuracy of local ancestry estimated by both the squared Pearson's correlation coefficient and the proportion of accurate local ancestry predictions (Methods). Across all software, the accuracy of local ancestry estimation consistently improves with increased reference sizes, irrespective of the admixture models with varying population counts (Fig. 3b and Supplementary Fig. 2).

In typical scenarios with smaller reference sizes (100 samples per local ancestry), FLARE exhibits marginally superior predictive performance, a trend that reverses (with these parameters) when there are over 1000 individuals per local ancestry. As anticipated, SparsePainter displays a negligible accuracy drop compared to ChromoPainter, given that SparsePainter is essentially a sparse implementation of ChromoPainter. Moreover, our results show a significant enhancement in accuracy when target individuals are sampled shortly post-admixture (after 3 generations, compared with 13) (Extended Data Fig. 1). Conversely, a reduction in SNPs correlates to diminished accuracy across all software, as seen in Supplementary Fig. 1.

Sparsity in SparsePainter

To investigate SparsePainter's tradeoff between sparsity and accuracy, we varied the reference size of a 5-way admixture model (Simulation 2c). Fig. 3c-d shows that a larger reference size substantially boosts accuracy, whilst increments in the number of matches only marginally elevate it, and larger reference samples dilute the accuracy's sensitivity to sparsity. Conversely, computational time and

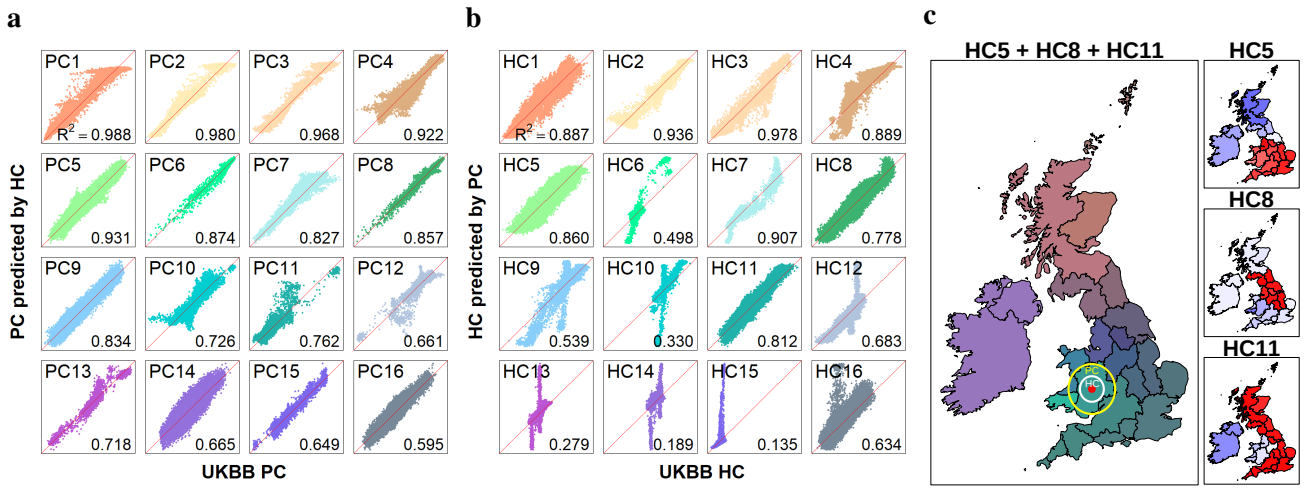

Fig. 4: **Comparison between UK Biobank PCs and HCs and the decomposition of HCs.** a, the coefficient of determination for predicting the first 16 UKB PCs (y-axis) using the first 150 HCs (x-axis) with linear regression models (n=406,733 individuals), which shows strong correlations. b, the coefficient of determination for predicting the first 16 UKB HCs (y-axis) using the first 150 PCs (x-axis) with linear regression models (n=406,733 individuals), which shows strong correlations on only 12 of the first 16 HCs. c, Visualisation of the average of the 5th, 8th and 11th HC stratified by birthplaces within the UK and Ireland (n=347,532 individuals), corresponding to the red, green, and blue channels, respectively, in the composite plot (left), and the right plot shows the decomposition of each HC. We have also shown the median prediction error range of the birthplace of HCs (white circle, radius 39.7km) and PCs (yellow circle, radius 77.5km) of an east Wales location (red point).

memory demands surge considerably as match density escalates. This indicates that if large reference datasets are available, opting for a constant number of matches (so diminished match proportion) yields significant computational savings, at a negligible compromise in accuracy.

Haplotype Principal Components Analysis for the UK Biobank

The UK Biobank (UKB)'s principal components (PCs) are widely used for correctly inferring the population structure. We inferred the (sparse) genome-wide pairwise coancestry of $N = 406,733$ UK Biobank individuals via PBWTpaint from $L = 569,242$ SNPs, taking 41 CPU hours (which is parallizable and scales as $O(NL)$). We summarised these ancestries into the top 150 haplotype components (HCs) (Methods), and compared their informativeness with PCs in several ways. First, we can accurately predict the first 16 PCs with the first 150 HCs using linear regression models (Fig. 4a), especially for the first 9 PCs which have a coefficient of determination (R^2) exceeding 80%. Conversely, when using the first 150 PCs to predict the first 16 HCs, some of the HCs are poorly explained (Fig. 4b). This observation indicates that HCs might encapsulate additional ancestry information beyond that conveyed by PCs.

To investigate consistency across chromosomes, we split the SNPs from the odd and even chromo-

somes and then computed the top 150 PCs and HCs from the even chromosome set. Subsequently, we used 150 HCs/PCs from one set to predict each of the top 50 HCs/PCs from the other set. HCs are well explained with $R^2 > 90\%$ for the majority of them (Extended Data Fig. 5), indicating HCs capture ancestry information that is shared in all the chromosomes. By contrast, few PCs can be predicted from different chromosome sets, which corresponds to the previous finding that all PCs except the top few of them are related to specific genetic regions[32].

HCs are associated with self-reported ethnicity (Extended Data Fig. 3): the 2nd and 3rd HCs effectively differentiate within white and black backgrounds, respectively, whereas the 4th and 6th HCs reflect variations associated with South Asian ancestry. HCs are also associated with geography: filtering to the 347,532 individuals with white, British or Irish ethnicity born in the UK or Ireland, we plotted the average HC for 23 UK regions (Extended Data Fig. 4). The 5th HC represents the variation between Scotland, Irish, and the rest of the UK, while the 11th HC differentiates Ireland and Wales from the other regions. By mapping the 5th, 8th, and 11th HCs onto the geography of the UK and Ireland, we created a colour-coded depiction (Fig. 4c) which uniquely identifies each county. Further, predicting birth location using HCs has a median error of 39.7km, whilst PCs give a nearly double error of 77.5km in out-of-sample individuals (see Methods). This is a surprisingly high accuracy as these individuals were not filtered for having ancestry from a single location, so prediction accuracy is bounded by migration since people need not be born where their ancestors came from.

Ethnicity-specific selection in the UK Biobank compared to the 1000 Genomes populations

To demonstrate the scientific value of SparsePainter, we inferred the local ancestry of 487,409 UK Biobank[33] individuals using the 2504 individuals spanning 26 populations from the 1000 Genomes Project (1000GP)[26] as reference. From this, we evaluated selection using LDA score, which quantifies genomic regions with particularly short ancestry segments, compared to the base recombination rate, as well as an Ancestry Anomaly Score (AAS), which quantifies regions of unusual ancestry, compared to genome-wide (see Methods). We report results that replicate over 7 primary self-reported ethnic backgrounds (hereafter ethnicities) within the UK Biobank: British, Irish, Indian, Caribbean, African, Pakistani, and Chinese. The LDAS, AAS and average probabilities of 26 1000GP populations for each SNP analysed within each ethnicity are available in Supplementary Tab. 2-8.

Naturally, admixture estimates vary between individuals from different ethnicities (Fig. 5a, Methods), but our goal is to demonstrate applications of local ancestry at scale outside of population history. We look for signals of 'putative selection' in the form of low LDAS and unusual AAS that are shared, i.e. identified in every UKB primary ethnicity (Methods). As a sensitivity analysis, we further painted the UK Biobank with 1000GP data using 5 continental ancestries (EUR, AFR, SAS, EAS and AMR). The LDAS and AAS results of different UKB ethnicities are illustrated in Fig. 5b-c. These are mapped to genes, with shared significant low LDAS and AAS signals visualised in Fig. 6 and investigated in detail in Supplementary Note 1. Genes with ethnicity-specific AAS signals are reported in Supplementary Tab. 1.

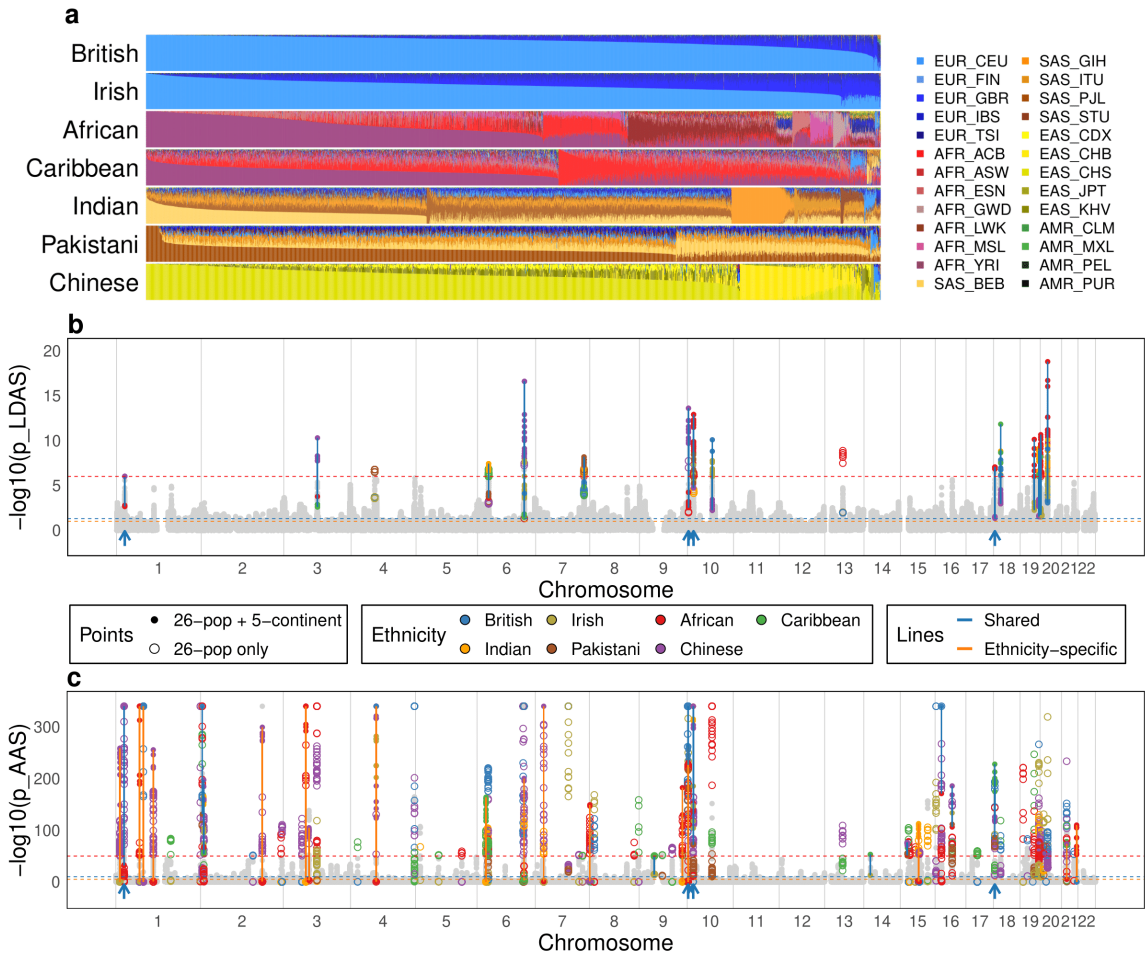

Fig. 5: **Modelling of 7 UK Biobank self-reported ethnicities using 26 1000GP populations.** a, Overall ancestry inference stratified by UKB ethnicities. For each ethnicity, the column shows ancestry decomposition for a single individual, with colours representing different 1000GP reference populations, named as regions followed by local population in standard abbreviation[26]. b, Linkage-Disequilibrium of Ancestry Score (LDAS), reporting -log10 of the p-value of low LDAS (normality test). c, Ancestry Anomaly Score (AAS) as a function of genome position, reporting -log10 of the p-value of AAS (chi-squared test). All plots describe the analysis of n=487,409 individuals on 569,242 SNPs. In b-c, the non-light-grey points (light grey points) represent the SNPs' maximum and minimum values that exhibit significant (insignificant) scores in both (either) paintings with 1000GP 26 populations and 5 continents, respectively (Methods), and blue (orange) lines connect the maximum and minimum values at each SNP that are shared (ethnicity-specific) across the 7 ethnicities in both paintings. The thresholds used to determine significance are depicted as horizontal lines in dashed red, blue and orange, respectively.

To aid in interpreting these signals, we extended simulations for low LDAS from Barrie et al. (2024)[12] (Methods, Extended Data Fig. 7-8). Two scenarios produce significantly low LDAS and extreme AAS, and both imply a change in selection following admixture. One scenario is single-locus

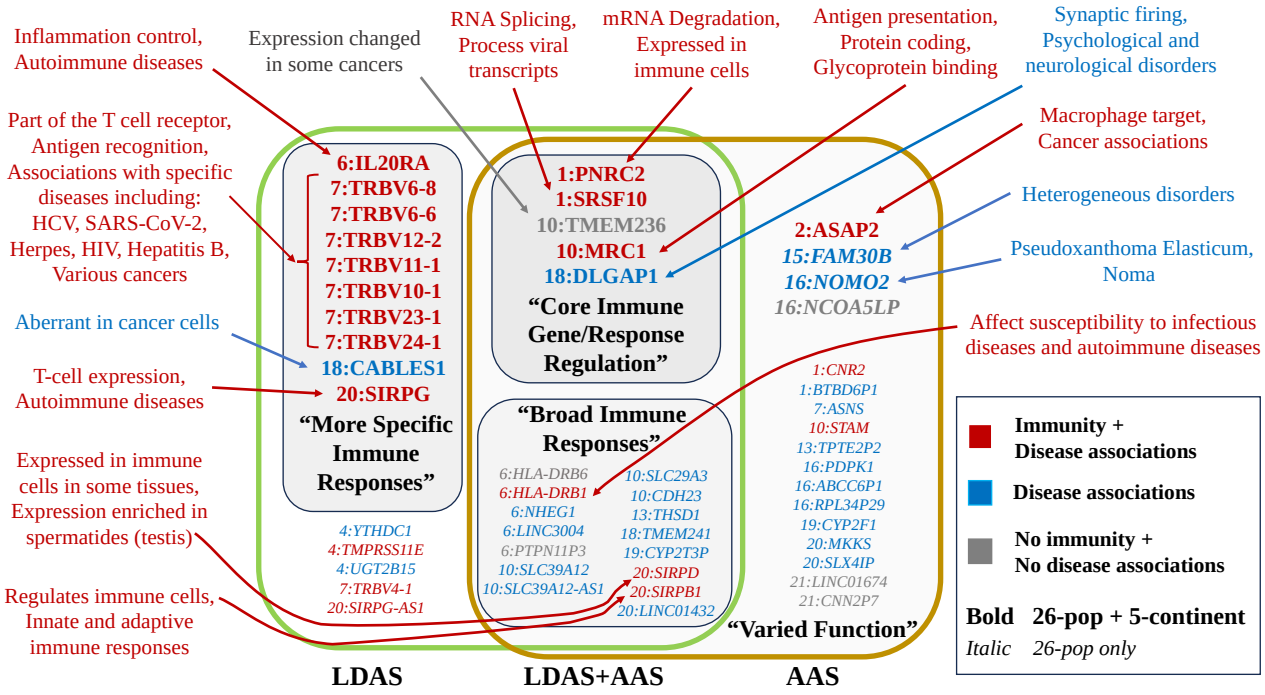

Fig. 6: **Summary of previous findings for genes with low LDAS and AAS signals shared between 7 UK Biobank self-reported ethnic backgrounds.** Genes with low LDAS and AAS signals in both 26-pop and 5-continent paintings include those with core immune gene or response regulation, while those in 26-pop painting only include many broad-impact immune genes. Genes with LDAS-only signals in both 26-pop and 5-continent paintings more typically affect responses to specific infections, and genes with AAS-only signals have varied functions and disease associations. Classification (colour) and category summaries (bold quoted text) are based on heuristic features of previous work; see Supplementary Note 1 for details.

negative selection in the admixed population, following non-negative selection in the pre-existing populations. The second scenario is multi-locus positive selection in the admixed population, while those loci are either absent or present at low frequency in some of the pre-existing populations. Selection under these scenarios is not detected by iHS, iHH12 or nSL as calculated using selscan[34], showing that extreme LDAS SNPs are not expected to be previously reported as under selection.

Extreme AAS signals in all 7 UKB ethnicities (Extended Fig. 9) include LINC01432 from chromosome 20 (linked to retroperitoneum carcinoma and early-onset androgenetic alopecia) which has an exceptionally high Japanese ancestry (EAS_JPT) across all UKB ethnicities. Similarly, in the genes PNRC2 and SRSF10 on chromosome 1, the Puerto Rican ancestry (AMR_PUR) is over-represented, particularly within European and Asian ethnicities. Notably, LINC03004 (highly expressed in testis and the gall bladder) and its nearby gene PTPN11P3 on chromosome 6 are predominantly represented by African ancestry across all ethnicities, a striking example of which is seen in Chinese ethnicity, where LINC03004 is almost completely African.

We observed that the different selection patterns of genes associated with the immune system were related to distinct hierarchies of control of immune response, from control of gene expression to T cell receptor recognition and inflammation. At the core were genes with low LDAS and AAS signals in both the 26 population ancestries and the 5 continental ancestries. These genes affect RNS degradation (PNRC2) and RNA splicing (SRSF10), and include a receptor that binds high-mannose structures on the surface of potentially pathogenic viruses, bacteria, and fungi (MRC1). The product of these genes affects immune responses (Supplementary Note 1.1), but their function is also central to non-immune pathways, and mutations in these genes can give rise to, for example, various congenital disorders and neurological and metabolic diseases.

The second level of control is broad-impact immune genes with low LDAS and AAS signals only in the (more recently separated) 26 population ancestries. The product of these genes affects antigen presentation and the strength of receptor signalling. One of the genes (HLA-DRB1) presents antigens to T cells and helps regulate immune responses. Over 2000 variants of DRB1 have been identified[35], some of which are associated with certain diseases or conditions (autoimmune diseases and susceptibility or protection infection). Whilst HLA-DRB6 is a pseudogene with, as of now, no known function, SIRPB1 encodes a signal-regulatory-protein that interacts with TYROBP/DAP12, a transmembrane adaptor protein on natural killer (NK) cells, peripheral blood monocytes, macrophages, dendritic cells, osteoclasts, and microglia. Through this interaction, SIRPB1 is involved in regulating both adaptive and innate immune responses and other pathways.

The least-central control level primarily affects responses to specific infections (T cell recognition, signalling) or localized responses that occur at the site of infection (inflammation), and have low LDAS scores but no AAS signals. Among them are eight less-commonly expressed TRBV genes, which are noteworthy for well-established associations with globally widespread and ancient herpesviruses, bacteria, and old pathogens such as hepatitis virus B and C, and influenza[36]. The TRBV genes encode part of the beta chain, which, together with the alpha chain (encoded by TRAV), form the T cell receptor's antigen binding site. Notably, 8 TRBV but no TRAV genes are identified. SIRPG is a signal-regulatory protein (SIRP) member and is involved in the negative regulation of receptor tyrosine kinase-coupled signalling processes. It affects the signal regulatory protein gamma (SIRPγ) expression on T-cells and helps regulate immune responses, cell adhesion, and phagocytosis. IL20RA mediates the pro-inflammatory effects of IL-20 cytokines, helps to regulate immune responses, tissue homeostasis, and inflammation, and is a central player in the immune system. TMPRSS11E affects epithelial barrier function, inflammation and wound healing. Conversely, only two genes out of the 16 with only an AAS signal are associated with the immune system, as the CNR2 gene product has anti-inflammatory effects, among other non-immune related functions, and PDK1 is a key regulator of immune cell development and function.

Discussion

Local ancestry inference is fundamental to understanding the genetic history of admixed populations, and fundamentally all populations are admixed. Our study presents highly efficient tools for performing ancestry inference that, in comparison with contemporary tools, substantially enhance computational efficiency while retaining inference accuracy. Our results showed that while increasing the reference panel size considerably improves the accuracy of local ancestry estimates, increasing the match density has diminishing returns on accuracy. This observation enables efficient fine-scale haplotype analyses for large-scale projects that aim to paint thousands or even millions of individuals, such as the UK Biobank and the larger biobanks of the future.

While our study has spotlighted the strengths of SparsePainter and PBWTpaint, it is also important to consider the scenarios where they might not be the optimal tool. For local ancestry estimation with few local ancestries, FLARE might offer a slight edge in terms of accuracy with comparable speed and memory usage, and MOSAIC offers a two-stage HMM that allows reconstruction of ancestries from imperfect reference panels. Conversely, while PBWTpaint shows remarkable efficiency in the genome-wide ancestries' estimation under *reference-vs-reference* painting, it is essential to note that it is designed for the specific purpose of identifying genome-wide patterns of ancestry sharing, which are of value for unsupervised clustering or making low dimensional summaries (HCs), but is not accurate at the level of local ancestry.

This work's broad implications extend beyond just technical improvement. The haplotype components (HCs) computed using PBWTpaint allow robust prediction of principal components (PCs) and may capture subtle genetic variations that PCs overlook - e.g. we found improved birthplace prediction performance within the UK Biobank. Haplotype summaries have other desirable properties such as not being associated with particular genomic regions, so replacing PCs with HCs is likely to result in a similar improvement as with ancestry components (ACs)[30], which require comparison to a reference panel as SparsePainter is designed for. We therefore left a thorough examination of this task to future work and focused on the visualisation of population genetic structure using HCs at scale.

We presented a more in-depth exploration of two measures of selection at the ancestry level - LDAS which identifies ancestry segments that are too short (or too long), and AAS which identifies regions with unusual ancestry patterns. We have been careful to treat these as 'putative selection' when interpreting them because there are other reasons for these anomalies to occur. LDAS and AAS would be sensitive to SNP density, long repeats, regions with many low-quality reads, or other structural issues. AAS is particularly sensitive to the makeup of the reference panel, which must be 'less admixed' than the target individuals on average to obtain a signal. LDAS is also sensitive to recombination map details (though the recombination rate for each ethnicity is separately normalised). Although (as we have attempted) such issues are typically removed in quality control or by post-hoc considerations (low data volume regresses to the prior genome-wide ancestry), we know of no other methods that can confirm these types of selection on this timescale.

AAS has previously linked infection in admixed Scottish wildcat *Felis silvestris* to selectively retain

an immune response developed in domestic cats *Felis catus*[37] over just 10 generations. Here, without looking specifically for it, we found many strong signals for core immune genes for all ethnicities using LDAS and AAS signals in the UK Biobank, which can be explained if there was a change in selection when these modern populations were formed as a mixture from older populations. Dating each would be very valuable - the admixture is only hundreds of years old for the African and European admixture seen in Afro-Caribbeans, and the last few thousand years for established populations described by 26 inter-continental populations from the 1000 Genomes Project. This historical timescale is consistent with the continued expansion of populations and their pathogens around the globe and implies a 'melting pot' of diverse diseases that evolved locally, likely related to environmental and cultural factors[38] and spread into global impact. For example, two selected immune genes (MRC1 and STAM) which have higher South Asian ancestries than expected facilitate the entry of the dengue virus, which is estimated to have evolved approximately 500-1000 years ago and first became endemic in parts of South and South-East Asia[39,40]. Today, it is widespread globally, and its range continues to expand as global warming increases the mosquito habitat that carries the dengue virus. It remains to be seen if the signal we see is this or some older virus that affects a related immune response.

Our analysis suggested that varying genetic selective patterns prevailed at different levels of control of a hierarchical complex biological system such as the immune system. Using these methods with carefully constructed reference panels targeting particular admixture times, and the analysis of specific contact events, could eventually build the pathogenic landscape around the world, and bring insights into more diseases and traits selected in our recent ancestors.

Methods

Modes of SparsePainter and PBWTpaint

There are three modes of SparsePainter and one mode of PBWTpaint as below. The painting with a leave-one-out strategy (as required for GLOBETROTTER[1] and related methods) is classified as panel painting, which is only possible for SparsePainter.

(1) all-vs-all. Under this mode, we paint each individual against all the other individuals, i.e. only the individual itself is left out. This is for clustering, computing HCs, or similar tasks. PBWTpaint has the best performance of speed and can only operate in this mode.

(2) *reference-vs-reference* painting with $npop$ populations. One individual is left out of each other population and oneself is left out from the own population. Then we paint a reference panel against itself. This 'panel painting' is for making a palette for each of the $npop$ populations as required for GLOBETROTTER[1], NNLS, and related admixture estimation methods. SparsePainter is efficient for this.

(3) *target-vs-reference* with $npop$ populations. We paint target individuals using a reference panel. We can either leave-one-out (one individual is left out of each population) or not. With leave-one-out, we can do admixture inference as the target is exchangeable with the reference. Without leave-one-out,

we can do local ancestry inference. SparsePainter is efficient for this.

Algorithm 'ReportLongestMatches'

The code implementation of the PBWT structure in SparsePainter drew extensively form Sanaullah et al. (2021)[24]. We extend the 'long match query' algorithm of PBWT in Algorithm 'ReportLongest-Matches' which aims to find at least Q longest matches at each position for a target sample i, in a two-stage process. In stage 1 we ensure a minimum number of matches, by storing only matches of length L_{min} or longer containing SNPs with fewer than Q matches in a set $\{s\}$. For efficiency, we search the longest matches first, by iteratively halving the match length L_q, beginning from L_0. For every SNP that still has fewer than Q matches, all matches longer than L_q containing the SNP are added to $\{s\}$, until all positions have at least Q matches or the halved length falls below L_{min}.

Stage 2 reduces the number of matches. First, we calculate the genetic length for each match in $\{s\}$ and sort them in descending order of their genetic lengths. An empty set $\{e\} = \emptyset$ is then populated with only the required matches. The algorithm traverses through the sorted $\{s\}$, adding a match to $\{e\}$ if any of its positions have fewer than Q matches in $\{e\}$. The final set $\{e\}$, containing elements that each specify the start position, end position, and reference sample number, represents the selected long matches to the reference haplotypes for the target sample i.

The efficiency of this algorithm is reflected by the majority of the genome being processed in Stage 1 with few long matches, even though there are huge numbers of matches throughout the genome. Subsequently, we only need to proceed to search relatively short sections of genomes for few relatively short matches.

Note that because of the limitation of L_{min}, we may end up having fewer than Q matches or even no matches at specific positions. The former doesn't decrease the accuracy of local ancestry inference, and we will address the latter in Methods – hidden Markov model.

Hidden Markov model in vector form

Let N be the number of haplotypes in the reference panel, and K be the number of SNPs. Also, we assume μ is the mutation probability per Morgan, and λ is the recombination scaling constant. The reference panel X is an N by K matrix, and a target haplotype y is an K-vector, all taking values of either 0 or 1 corresponding to whether the reference allele is present or not. However, we can simplify this into a **match matrix** M of dimension $N \times K$ which also takes values of either 0 or 1, with $M_{ij} = 1$ if $X_{ij} = y_j$ and 0 otherwise. We will refer to the row vectors $\mathbf{m}_j = M_{\cdot j}$ and use the shorthand $D(\mathbf{x}) = \mathrm{Diag}(\mathbf{x})$ as the matrix with the vector $\mathbf{x}$ on the diagonal. We will refer to $D_N(x)$ as an $N \times N$ matrix with the scalar x on the diagonal.

SparsePainter implements the Li and Stephen's model[17] in the form of ChromoPainter[18] in a sparse setting. We define $\mathbf{V}$ as the emission matrix, and the column vectors are $\mathbf{v}_j = V_{\cdot j}$

$$\mathbf{V_{ij}} = \begin{cases} 1-\mu & \text{if } \mathbf{M}_{ij} = 1 \\ \mu & \text{if } \mathbf{M}_{ij} = 0 \end{cases} \tag{1}$$

Algorithm 1 ReportLongestMatches—-find at least Q Longest matches at each position for target sample i

Stage 1: Ensuring a minimum number of matches;

Run PBWT and record all matches longer than or equal to L_0 SNPs in set $\{s\}$.
Let $\mathbf{r}$ be a list of SNP indices with fewer than Q matches;
Iteration $q \leftarrow 1$ and current minimum length $L_q \leftarrow L_0/2$;
while $|r| \neq 0 \wedge L_q \geq L_{min}$ **do**
    Run PBWT and with min length L_q ;
    Add matches containing SNPs in $\mathbf{r}$ with length $\in [L_q, L_{q-1})$ to set $\{s\}$;
    Update $\mathbf{r}$ with the indices of SNPs with fewer than Q matches of length L_q or longer;
    Half the minimum match length L_q subject to constraints, i.e. $L_{q+1} \leftarrow \max(L_q/2, L_{min})$;
    $q \leftarrow q + 1$;
end while

Stage 2: Reduce the number of matches;

▷ *Retain only the longest, required matches.*

Compute the genetic distance of each match in set $\{s\}$ and store in $\{g\}$
Sort set $\{s\}$ in descending order of $\{g\}$;
Define $\{e\}$ as an empty set to record final selected matches;
for $b \leftarrow 1$ to $|s|$ **do**
    Add match $s[b]$ to set $\{e\}$ if it contains SNPs with fewer than Q matches;
    If all SNPs have at least Q matches **break**;
end for
Report $\{e\}$ as the selected long matches to reference haplotypes for target sample i.

The observation matrix is an $N \times N$ matrix:

$$\mathbf{O}_j = (1-\mu)D_N(\mathbf{m}_j) + \mu D_N(\mathbf{1}_N - \mathbf{m}_j) = D_N(\mathbf{v}_j) \tag{2}$$

The transition matrix from position j to position $j+1$ is an $N \times N$ matrix:

$$\mathbf{T}_j = \rho_j D_N(1) + \frac{1-\rho_j}{N}\mathbf{1}_{N\times N} \tag{3}$$

where $\rho_j = \exp(-\lambda g_j)$ with g_j being the genetic distance between position j and position $j+1$ in Morgans.

Let $f_0 = 1/N$ be the prior probabilities for the matches. We can write the forward probabilities for $j = 1, \ldots, K$ as:

$$\mathbf{f}_j = \mathbf{f}_{j-1}\mathbf{T}_{j-1}\mathbf{O}_j, \tag{4}$$

where $\mathbf{f}_j$ are row vectors ($1 \times N$). With $\mathbf{b}_K = \mathbf{1}_N$ where $\mathbf{1}_N$ is an $1 \times N$ row vector, the backward probabilities for $j = 1, \ldots, K-1$ are:

$$\mathbf{b}_j^T = \mathbf{T}_j \mathbf{O}_{j+1} \mathbf{b}_{j+1}^T. \tag{5}$$

However, Equation (4) and (5) can be significantly simplified due to the special form of the output and transition matrices. We can arrive at a **vector form** for which computations are $O(N)$ instead of $O(N^2)$.

To simplify notation, will write the marginal (partial) probabilities $\sum_{i=1}^N f_{ij} = \tilde{f}_j$ and $\sum_{i=1}^N b_{ij} = \tilde{b}_j$, the total number of matches $\tilde{m}_j = \sum_{i=1}^N m_{ij}$, as well as writing $\tilde{\rho}_j = \frac{1-\rho_j}{N}$. These are all scalar properties in what follows below. For the forward probabilities:

$$\begin{aligned}
\mathbf{f}_j &= \mathbf{f}_{j-1} \left[\rho_{j-1} D_N(1) + \tilde{\rho}_{j-1} \mathbf{1}_{N\times N}\right] \left[(1-\mu) D\left(\mathbf{m}_j\right) + \mu D\left(\mathbf{1}_N - \mathbf{m}_j\right)\right] \\
&= \mathbf{f}_{j-1}\rho_{j-1} \left[(1-\mu) D_N\left(\mathbf{m}_j\right) + \mu D\left(\mathbf{1}_N - \mathbf{m}_j\right)\right] + \tilde{f}_{j-1}\tilde{\rho}_{j-1}\mathbf{1}_N \left[(1-\mu) D\left(\mathbf{m}_j\right) + \mu D\left(\mathbf{1}_N - \mathbf{m}_j\right)\right] \\
&= (1-\mu)\mathbf{m}_j \circ \left[\rho_{j-1}\mathbf{f}_{j-1} + \tilde{f}_{j-1}\tilde{\rho}_{j-1}\mathbf{1}_N\right] + \mu \left[\rho_{j-1}\mathbf{f}_{j-1} + \tilde{f}_{j-1}\tilde{\rho}_{j-1}\mathbf{1}_N\right] \circ \left(\mathbf{1}_N - \mathbf{m}_j\right) \\
&= \mathbf{v}_j \circ \left[\rho_{j-1}\mathbf{f}_{j-1} + \tilde{f}_{j-1}\tilde{\rho}_{j-1}\mathbf{1}_N\right]
\end{aligned} \tag{6}$$

where we use the notation $\mathbf{x} \circ \mathbf{y}$ for entry-wise vector multiplication (Hadamard product). Similarly for the backward probabilities, using the shorthand $\mathbf{c}_j = \mathbf{m}_j \circ \mathbf{b}_j$ and $\sum_{i=1}^N m_{ij} b_{ij} = \tilde{c}_j$:

$$\begin{aligned}
\mathbf{b}_j^T =& \left[\rho_j D_N(1) + \tilde{\rho}_j \mathbf{1}_{N\times N}\right] \left[(1-\mu) D_N\left(\mathbf{m}_{j+1}\right) + \mu D_N\left(\mathbf{1}_N - \mathbf{m}_{j+1}\right)\right] \mathbf{b}_{j+1}^T \\
=& \rho_j \left[(1-\mu) D_N\left(\mathbf{m}_{j+1}\right) + \mu D_N\left(\mathbf{1}_N - \mathbf{m}_{j+1}\right)\right] \mathbf{b}_{j+1}^T + \\
& \tilde{\rho}_j \mathbf{1}_{N\times N} \left[(1-\mu)\left(\mathbf{m}_{j+1} \circ \mathbf{b}_{j+1}\right)^T + \mu \mathbf{b}_{j+1}^T \circ \left(\mathbf{1}_N - \mathbf{m}_{j+1}\right)^T\right] \\
=& \rho_j (1-\mu)\mathbf{c}_{j+1}^T + \rho_j \mu \left(\mathbf{b}_{j+1}^T - \mathbf{c}_{j+1}^T\right) + \tilde{\rho}_j (1-\mu)\tilde{c}_{j+1}\mathbf{1}_N^T + \tilde{\rho}_j \mu \left(\tilde{b}_{j+1} - \tilde{c}_{j+1}\right)\mathbf{1}_N^T \\
=& \rho_j \left(\mathbf{c}_{j+1}^T - 2\mu\mathbf{c}_{j+1}^T + \mu\mathbf{b}_{j+1}^T\right) + \tilde{\rho}_j \left(\tilde{c}_{j+1} - 2\mu\tilde{c}_{j+1} + \mu\tilde{b}_{j+1}\right)\mathbf{1}_N^T \\
=& \rho_j \mathbf{d}_{j+1}^T + \tilde{\rho}_j \tilde{d}_{j+1}\mathbf{1}_N^T
\end{aligned} \tag{7}$$

where $\mathbf{d}_j = \mathbf{v}_j \circ \mathbf{b}_j$ and such that $\sum_{i=1}^N v_{ij} b_{ij} = \tilde{d}_j$. Finally, the posterior probabilities are written in the following form:

$$P(\mathbf{m}_j | \mathbf{O}) \propto \mathbf{f}_j \circ \mathbf{b}_j^T. \tag{8}$$

If we assume the mutation rate $\mu \to 0$, the forward and backward probabilities (Equation (6) and (7)) simplify to

$$\mathbf{f}_j = \mathbf{m}_j \circ \left[\rho_{j-1}\mathbf{f}_{j-1} + \tilde{f}_{j-1}\tilde{\rho}_{j-1}\mathbf{1}_N\right] \tag{9}$$

and

$$\mathbf{b}_j^T = \rho_j \delta_{j+1}^T + \tilde{\rho}_j \tilde{\delta}_{j+1} \mathbf{1}_N^T \tag{10}$$

respectively, where $\delta_j = \mathbf{m}_j \circ \mathbf{b}_j$ and $\tilde{\delta}_j = \sum_{i=1}^{N} m_{ij} b_{ij}$. In this case, only the forward probabilities $\mathbf{f}_j$ for the matched samples at position j are non-zero and need to be calculated. For backward probabilities, we compute different $\mathbf{b}_j^T$ for matched samples at position $j+1$, with unmatched samples sharing the same default value $\tilde{\rho}_j \tilde{\delta}_{j+1}$ in the jth hash vector. Finally, when computing the posterior probabilities $P(\mathbf{m}_j|\mathbf{O})$ (Equation (8)), only samples with matches in SNP j or $j+1$ require computation, whereas the others are exactly 0.

Note that this assigns non-zero probability to single mutation breaks in haplotypes, provided a match is found both to the left and the right. In conclusion, the Hash-Map-based forward and backward algorithm reduces computational cost from $O(N)$ (e.g., ChromoPainter[18]) to approximately $O(Q)$.

There are instances when few positions have no matches spanning at least L_{min} SNPs, and are therefore interpreted as no matches, which disrupts the forward and backward algorithm because a 0-vector of $\mathbf{f}_j$ causes all $\mathbf{f}_t$ to become 0-vectors for any $t > j$. To address this issue, for each position without matches, we find the closest SNP (in genetic distance) that has matches. We then impute the matches from this closest SNP to the position without matches.

The recombination scaling constant λ is usually estimated by the Expectation–Maximization (E-M) algorithm (Supplementary Note 2.2). However, the Viterbi algorithm, a dynamic programming technique to identify the most probable sequence of hidden states in a hidden Markov model, can be advantageously employed to improve the efficiency of estimating λ, compared with the E-M algorithm. In this context, let N_{seg} represent the minimum number of contiguous segments from different reference samples required to construct the target haplotype, and therefore $N_{\text{break}} = N_{\text{seg}} - 1$ is essentially the number of distinct recombination events that have been inferred. Then λ is estimated as

$$\lambda^* = \frac{N_{\text{break}}}{\sum_{j=1}^{K} g_j}. \tag{11}$$

The normalised versions of the forward and backward equations

It is helpful to work in the normalised versions of the forward and backward equations $\check{\mathbf{f}}_j = \mathbf{f}_j / \tilde{f}_j$ and $\check{\mathbf{b}}_j = \mathbf{b}_j / \tilde{b}_j$. We define F_j and B_j as the normalising constant at state j.

$$\frac{\mathbf{f}_j}{\tilde{f}_{j-1}} = \mathbf{m}_j \circ \left[(1-\mu)\left(\rho_{j-1}\check{\mathbf{f}}_{j-1} + \tilde{\rho}_{j-1}\mathbf{1}_N\right) - \mu\left(\rho_{j-1}\check{\mathbf{f}}_{j-1} + \tilde{\rho}_{j-1}\mathbf{1}_N\right)\right] + \mu\left[\rho_{j-1}\check{\mathbf{f}}_{j-1} + \tilde{\rho}_{j-1}\mathbf{1}_N\right] \tag{12}$$

Setting $\mu \to 0$, $\mathbf{v}_j$ shrinks to $\mathbf{m}_j$:

$$\begin{aligned} \mathbf{f}_j &= \mathbf{m}_j \circ [\rho_{j-1}\mathbf{f}_{j-1} + \tilde{f}_{j-1}\tilde{\rho}_{j-1}\mathbf{1}_N] \\ \check{\mathbf{f}}_j &= \frac{\tilde{f}_{j-1}}{\tilde{f}_j}\frac{\mathbf{f}_j}{\tilde{f}_{j-1}} = \frac{\tilde{f}_{j-1}}{\tilde{f}_j}\mathbf{m}_j \circ [\rho_{j-1}\check{\mathbf{f}}_{j-1} + \tilde{\rho}_{j-1}\mathbf{1}_N] \\ &= \frac{1}{F_j}\mathbf{m}_j \circ [\rho_{j-1}\check{\mathbf{f}}_{j-1} + \tilde{\rho}_{j-1}\mathbf{1}_N] \end{aligned} \tag{13}$$

which has the following consequences:

(a) Let s_j be the set of matches at SNP j: $i \in s_j \iff m_{ij} = 1$.
(b) $\check{f}^*_{ij} = \rho_{j-1}\check{f}_{i(j-1)} + \tilde{\rho}_{j-1}$ if $i \in s_j$ and is zero otherwise.
(c) $F_j = \sum_{i \in s_j} \check{f}^*_{ij}$ and $\check{f}_{ij} = \check{f}^*_{ij}/F_j$.
(d) for a sparse algorithm, we only need to track matches and the relative sums of their probabilities.

For the backward algorithm with $\mu \to 0$, $\mathbf{d}_j$ shrinks to $\mathbf{c}_j$:

$$\begin{aligned} \mathbf{b}_j^T &= \rho_j \mathbf{c}_{j+1}^T + \tilde{\rho}_j \tilde{c}_{j+1} \mathbf{1}_N^T \\ \check{\mathbf{b}}_j^T &= \frac{\tilde{c}_{j+1}}{\tilde{b}_j} \left[\rho_j \check{\mathbf{c}}_{j+1}^T + \tilde{\rho}_j \mathbf{1}_N^T\right] \end{aligned} \tag{14}$$

which has the following consequences:
(a) $\check{b}^*_{ij} = \rho_j \check{b}_{i(j+1)} + \tilde{\rho}_j \tilde{c}_{j+1}$ if $i \in s_{j+1}$ and $\check{b}^*_{ij} = \tilde{\rho}_j \tilde{c}_{j+1}$ otherwise, where $\tilde{c}_{j+1} = \sum_{i \in s_{j+1}} b_{i(j+1)}$.
(b) $B_j = \sum_{i \in s_{j+1}} \check{b}^*_{ij} + (N - n_{j+1})\tilde{\rho}_j \tilde{c}_{j+1}$ and $\check{b}_{ij} = \check{b}^*_{ij}/B_j$.
(c) Again this can be computed without explicit reference to non-matches and we need to sum over only matches.

Estimation of the expected length of copied chunks

Let $\hat{l}_i$ denote the posterior expected length (in Morgans) of the total genome for which the sample haplotype copies from the ith reference haplotype.

$$\begin{aligned} \hat{l}_i =& \frac{1}{2\Pr(D)} \sum_{j=1}^{K-1} g_j \left[f_{ij} b_{ij} + f_{i(j+1)} b_{i(j+1)}\right] \\ =& \frac{1}{2\prod_{k=1}^K F_k} \sum_{j=1}^{K-1} g_j \left[\check{f}_{ij}\check{b}_{ij}(\prod_{k=1}^{j} F_k)(\prod_{k=j}^{K} B_k) + \check{f}_{i(j+1)}\check{b}_{i(j+1)}(\prod_{k=1}^{j+1} F_k)(\prod_{k=j+1}^{K} B_k)\right] \\ =& \frac{1}{2} \sum_{j=1}^{K-1} g_j \left[w_j^l \check{f}_{ij}\check{b}_{ij} + w_j^r \check{f}_{i(j+1)}\check{b}_{i(j+1)}\right] \end{aligned} \tag{15}$$

where

$$w_j^l = \exp\left(\log(\prod_{k=1}^{j} F_k) + \log(\prod_{k=j}^{K} B_k) - \log(\prod_{k=1}^{K} F_k)\right)$$

and

$$w_j^r = \exp\left(\log(\prod_{k=1}^{j+1} F_k) + \log(\prod_{k=j+1}^{K} B_k) - \log(\prod_{k=1}^{K} F_k)\right).$$

Non-negative Least Squares (NNLS) for admixture estimation

Admixture estimation can be performed on both the reference individuals and the target individuals via NNLS, which requires the expected total genome shared between each reference ancestry, and each reference (or target) individual with each reference ancestry. The former is derived by painting the

reference samples against themselves with one sample left out of each other population (i.e. *reference-vs-reference* painting). We then average each reference individual within each reference population to provide a reference palette. When investigating admixture estimation for target individuals, we also require painting each target sample (i.e. *target-vs-reference* painting) against a reference panel, with one sample left out from every reference population. Reference (target) samples are then described as a mixture of the reference populations using NNLS, calculated by the R package 'nnls' [1].

Simulation details for comparison between SparsePainter, PBWTpaint, ChromoPainter and FLARE

We simulated different simple models (Simulation 2a-c) for *target-vs-reference* painting, and a hierarchical model (Simulation 1) for *reference-vs-reference* painting. Each simulation is repeated 10 times, and the average statistics, i.e. compute time, memory usage and accuracy, are reported.

The simple simulation model for *target-vs-reference* painting (Simulation 2a-c) begins with an ancestral population that evolves for 2500 generations prior to diverging into n_{pop} populations. Following an evolutionary period of another 500 generations, these n_{pop} populations undergo admixture, culminating in a modern population, and the target individuals are sampled T generations after admixture. The simulation spans 100 megabases (Mbs), characterized by a mutation rate of 6×10^{-9} per base pair per generation, and a recombination rate of 2×10^{-8} Morgans per base pair per generation.

The true local ancestry is defined as 1 generation before admixture, which is derived from the recombination events recorded in the tree sequences (in SLiM) during the 500 generations. There are some regions (around 10% to 20%) in target haplotypes that are inherited from the ancestral population and haven't experienced any recombination events during the 500 generations. For comparing the local ancestry estimates, we excluded the SNPs within those regions, while for inferring the genome-wide total ancestry for comparison of NNLS estimates, we assumed those regions without recent recombination events have the same proportion of total ancestries as the other regions.

We also constructed a hierarchical model (**Simulation 1**) that mirrors the evolutionary trajectory of real-world populations, which is used for the comparison of *reference-vs-reference* panel painting. In detail, we simulated 5 populations $P_i(i = 1, 2, ..., 5)$ as below: After evolving for 2933 generations, an ancestral population split into P_1 and P_4. After generation 2958, P_2 emerged from migrations originating from P_1. Moving forward to the 2983th generation, some people from P_2 migrated to a new population P_3. A final migration occurred at the 2993th generation when some individuals from P_4 settled to create P_5. After 3000 generations, we sampled an equivalent number of individuals (ranging from 10 to 500) from each population $P_i(i = 1, 2, ..., 5)$. A similar model was constructed for simulating 10 hierarchical populations. We used the same procedures to define the true genome-wide total ancestry as above.

For all the simulations, we retained a fixed number of common SNPs with Minor Allele Frequency (MAF) of at least 0.5% from the reference and target datasets, which are presented in the Variant Call Format (VCF). There datasets were then merged. Subsequently, we phased the merged dataset with Beagle 5.4[41] before splitting it into the reference and target datasets. FLARE requires input data in the

VCF format, while SparsePainter and ChromoPainter require the phase format, which can be converted from VCF efficiently using the PBWT software.

For SparsePainter, unless otherwise stated, we ensured no more than 10 longest matches (longer than 20 SNPs) at each locus are retained. All simulations are performed on an MSI laptop with an Intel Core i7-10750H processor running at 2.60GHz on 10 CPU cores in parallel.

We explored a number of different parameters for Simulation 2a-c.

- **Simulation 2a**: we simulated 2-, 5-, 10-, 20-, 40-, 50-, 80- and 100-way admixture ($npop = 2$, 5, 10, 20, 40, 50, 80, 100) to compare the speed and memory between software, with varying numbers of total reference sizes (2000, 4000 or 8000), and varying numbers of target individuals (100 or 500) with 2100 SNPs.
- **Simulation 2b**: we simulated 2-, 3- and 5-way admixture ($n_{pop} = 2$, 3 or 5) to compare the accuracy between software, with varying number of reference sizes for each reference ancestry (from 100 up to 2000), number of SNPs ($K = 1800$ or 3600) and evolving time of 50 modern individuals ($T = 3$ or 13). The admixture proportion is (50%,50%) for 2-way, (20%,50%,30%) for 3-way, and (20%,10%,10%,40%,20%) for 5-way models, respectively.
- **Simulation 2c**: we drew from reference pools of 5000, 10000, or 20000 individuals from $n_{pop} = 5$ local ancestries consisting of 5000 SNPs. We then evaluated SparsePainter's efficiency in painting 1000 individuals who are sampled 13 generations after admixture under varying levels of sparsity, i.e. only the longest 5, 10, 20, 40 and 80 matches which are longer than 20 SNPs are retained at each SNP. This was manipulated via the 'nmatch' parameter in SparsePainter.

Methods to evaluate the accuracy of local ancestry and NNLS estimates

We used two different methods to assess the accuracy of local ancestry estimates. The first method is the squared Pearson's correlation coefficient (denoted as r^2). At each SNP, we calculated the estimated dosage of each individual by averaging the posterior probabilities of both haplotypes for each reference ancestry, and the true dosage is the average true local ancestry which takes values of 0, 0.5, or 1.

We computed the r^2 between the estimated and actual dosages for each reference ancestry across all individuals and positions, and the unweighted mean r^2 of these values is reported to measure the overall accuracy. The second method evaluates the proportion of accurate local ancestry predictions across all haplotypes and positions. For each haplotype at a given position, a correct local ancestry inference is determined when the true local ancestry corresponds to the highest estimated posterior probability.

To evaluate the accuracy of admixture estimation, we calculated the squared correlation between the NNLS-estimated coefficient and the true proportion for all the individuals, and reported the unweighted mean r^2 of NNLS from different local ancestries.

The accuracy of PBWTpaint for local ancestry estimation

We assessed the accuracy of PBWTpaint for local ancestry inference under *reference-vs-reference*

panel painting by comparing its Pearson's squared correlation with SparsePainter. On the simple simulation model (Simulation 2-4) in which the ancestries are distinct, the r^2 between PBWTpaint and SparsePainter is high at 0.79. However, for complex cases in which there is uncertainty, or the true ancestry is an ancestor of extant populations (Simulation 1), the set maximal matches used by PBWTpaint lead to over-confident or inaccurate local ancestry assignment ($r^2 = 0.3$) even though these mistakes are self-averaging for the estimation of genome-wide ancestry. This illustrates that PBWTpaint is not an appropriate method for performing local ancestry estimates.

Simulation for LDAS under genetic drift

We assessed the robustness of the LDAS and its sensitivity to demographic changes by examining it under genetic drift across exponentially expanding population sizes over time. We simulated a genome of a 500Mb region as follows: initially, an ancient population evolves for 1000 generations, subsequently diverging into five distinct subpopulations. Each of these subpopulations, growing at a rate of 2% per generation, evolves independently for 100 generations. This period of divergence is followed by a phase of admixture, forming a modern, unified population, which then undergoes evolution for an additional 30 generations at an increased growth rate of 5% per generation.

We computed the LDAS of 500 simulated modern individuals with 2000 simulated reference individuals from each of the 5 subpopulations. After normalisation, the z-scores of the LDAS (Extended Data Fig. 6a) predominantly exhibit under-dispersion, despite some noticeable deviation on both tails. This pattern suggests that the normal distribution is a reasonable approximation for the LDAS distribution. Subsequently, we calculated the p-values for low LDAS through a one-sided test for normality, as depicted in Extended Data Fig. 6b. Notably, no low LDAS signals are detected under the genetic drift model (excluding selection effects), as evidenced by the most significant SNP with $p < 10^{-3}$. This outcome solidifies our conclusion that low LDAS signals are not present under this model.

Simulation for comparing LDAS with statistics for positive selection

Here we simulated the similar two-loci and one-locus model as used in Barrie et al. (2024)[12].

For the two-loci selection model (Extended Data Fig. 7), we simulated a genome of 150Mb. Initially, an ancient population evolved for 2200 generations before splitting into two sub-populations $P1$ and $P2$. After evolving 400 generations, we added mutation $m1$ for $P1$ and $m2$ for $P2$ at locus 20Mb and 23Mb, respectively. These added mutations were then positively selected in the following 300 generations before admixing to $P3$ at generation 2900. $m1$ and $m2$ then experienced strong positive selection for another 50 generations, after which we sampled 500 individuals from $P3$ as target individuals. 500 individuals are sampled for $P1$ and $P2$ at generation 2899 as the reference panel.

For the one-locus selection model (Extended Data Fig. 8), we simulated a genome of 50Mb. The remaining difference from the above mode is that only one locus $m0$ at 20Mb was added at generation 2601 for both $P1$ and $P2$, and it was positively selected until generation 2900. In the admixture population $P3$, this SNP underwent negative selection until generation 2950 when the target individuals

were sampled.

Paint all UK Biobank individuals against themselves and calculate haplotype principal components

To infer the haplotype principal components, we painted UKB biobank individuals against themselves, i.e. *all-vs-all* painting. We first excluded related individuals as described by Bycroft et al. (2018)[33] and excluded withdrawn individuals. We then performed PBWTpaint (with command pbwt -paintSparse) on each chromosome of UK Biobank phased genotype data, which in total has 406,733 individuals with approximately 569,242 SNPs. The total chunk length of PBWTpaint for each individual on chromosome i is $2K_i$, where K_i is the number of SNPs. Assume g_i is the total genetic distance for chromosome i, we weighted the chunk length for chromosome i with weight g_i/K_i. Then we summed up the sparse chunk length matrix for all the chromosomes as matrix A, such that for each individual (i.e. each row of A), the expected lengths of copied chunks from all other individuals reached the sum of the total genetic distance $G = \sum_{i=1}^{22} g_i$.

We performed singular value decomposition (SVD) on the log-transformed sparse chunk length matrix $log10(A+1)$ with R package 'sparsesvd': $log10(A+1) = UDV^T$, where D is a diagonal matrix of the singular values. Then we extracted the the first 150 columns of $U\sqrt{D}$ as the top 150 haplotype principal components.

Prediction of birth locations with HCs and PCs

We conducted an analysis to evaluate the predictive accuracy of Haplotype Components (HCs) and Principal Components (PCs) on the birth locations, i.e. the east and north coordinates, within the UK. We selected a cohort of 347,532 individuals who were born in the UK or Ireland and identified as white, British, or Irish ethnicity. This cohort was divided into two groups: a training set comprising 80% of the individuals, and a test set consisting of the remaining 20%. Subsequently, with either the top 150 PCs or HCs as explanatory variables and either the east or north coordinate as the response variable, we used a 5-fold CV to determine the optimal number of boosting iterations before fitting the regression model on the training set with eXtreme Gradient Boosting (XGBoost[42]), and then we predicted the birth coordinates of individuals in the test set. Finally, we computed the direct distance between the predicted coordinates and the actual coordinates of each individual on the test set and reported the median which reveals that using HCs as predictors (median error=39.7km) reduced 49% error compared with using PCs as predictors (median error=77.4km). This indicates a notably higher predictive accuracy of birthplaces when using HCs.

Paint UK Biobank with 1000 Genomes Project

We inferred the local ancestry of UK Biobank individuals using the 1000 Genomes Project (1000GP) as the reference data, which includes 2504 individuals from 26 populations. We retained the common bi-allelic SNPs with $\mathrm{MAF} \geq 5\%$ before merging these two datasets. Then we used Beagle 5.4[41] to phase

the merged dataset, after which it was split into the reference and target datasets. For a comparative analysis of the genetic painting and population structure within the UK Biobank, we randomly selected 10,000 individuals with self-reported British backgrounds, and incorporated all individuals from specific self-reported ethnic backgrounds: Irish (12713), Indian (5660), Caribbean (4297), African (3203), Pakistani (1747), and Chinese (1503).

We estimated the average recombination scaling constant $\lambda = 164.2$ of all these individuals on chromosome 19. This fixed parameter was subsequently used for painting across chromosomes 1-22. Besides, to achieve higher accuracy, we configured the parameters of SparsePainter to aim for finding the 50 longest matches (longer than 20 SNPs) at each position.

Shared and ethnicity-specific LDAS and AAS

Here we explain the methods for finding shared and ethnicity-specific LDAS and AAS. As introduced by Barrie et al. (2024)[12], we computed the LDAS of SNP j in a $X = 4\text{cM}$ window $\text{LDAS}(j; X)$ by:

$$\text{LDAS}(j;X) = \begin{cases} \int_{g(j)-X}^{g(j)+X} \text{LDA}(j,l)\,dg & \text{if } X \le g(j) \le tg - X, \\ \int_{0}^{g(j)+X} \text{LDA}(j,l)\,dg + \int_{2g(j)}^{g(j)+X} \text{LDA}(j,l)\,dg & \text{if } g(j) < X, \\ \int_{g(j)-X}^{tg} \text{LDA}(j,l)\,dg + \int_{g(j)-X}^{2g(j)-tg} \text{LDA}(j,l)\,dg & \text{if } g(j) > tg - X. \end{cases} \tag{16}$$

where tg is the total genetic distance in centiMorgan, and $\text{LDA}(j,l)$ is the LDA between SNP j and l.

One major source of bias in the estimate of LDAS is due to sparse SNP sampling, as the LDA score is calculated by summing the space under piecewise linear functions. To handle this without making further distributional assumptions, we propose a quality control method.

An upper bound and lower bound of the estimates of LDAS can be obtained by replacing the linear interpolation in Equation 16 with a step function. In detail, we take the larger and smaller LDA values of two neighbouring SNPs, respectively, as the fixed LDA in the genetic distance between the two SNPs in the integral over the XcM-window on both sides of the SNP. Specifically:

$$\text{LDA}_{\text{upper}}(j,l) = \max\left\{\text{LDA}(j,l), \text{LDA}(j,l+1)\right\}$$

and

$$\text{LDA}_{\text{lower}}(j,l) = \min\left\{\text{LDA}(j,l), \text{LDA}(j,l+1)\right\},$$

which can be substituted into Equation 16 to obtain an upper and lower-bound respectively of the LDAS of SNP j: $\text{LDAS}_{\text{upper}}(j;X)$ and $\text{LDAS}_{\text{lower}}(j;X)$. When computing $\text{LDAS}_{\text{lower}}(j;X)$, we assume $\text{LDA}(j, g=0) = \text{LDA}(j, g=td) = 0$ for conservative estimation.

Intuitively, the maximum possible error of LDAS of SNP j is

$$\text{LDAS}_{\text{error}}(j;X) = \text{LDAS}_{\text{upper}}(j;X) - \text{LDAS}_{\text{lower}}(j;X). \tag{17}$$

However, the LDAS are in different scales across different ethnic backgrounds, because of different admixture times. Therefore, for each ethnic background, we normalise the $\text{LDAS}_{\text{error}}$ with the average

LDAS across the genome, i.e. $\mathrm{LDAS}^*_{\mathrm{error}} = \mathrm{LDAS}_{\mathrm{error}}/\mathrm{E}(\mathrm{LDAS})$, and then we remove SNPs with $\mathrm{LDAS}^*_{\mathrm{error}} \geq \delta$ where δ is a specified threshold (we used $\delta = 0.3$).

However, the above method cannot entirely alleviate the impact of regions in sparse. In practice, the pairwise LDA shrinks to almost 0 when the closest SNPs are more than 3 centiMorgan (cM) away. We therefore removed SNPs in very sparse regions based on their 3cM windows: SNP j is removed if at least one of $n_m(j) < \theta$ for $m = 0.5, 1, 1.5, 2, 2.5, 3$, where $n_m(j)$ is the number of SNPs that is $(m - 0.5, m]$cM away from SNP j and θ is a specified threshold (we used $\theta = 10$).

In conclusion, we used the hybrid of $\mathrm{LDAS}_{\mathrm{error}} < \delta$ and $n_m \geq \theta$(m=0, 0.5, 1.0, 1.5, 2, 2.5) as the quality control of SNPs, which alleviates the bias estimates due to sparsity of the painting data and therefore avoids extreme LDA scores.

The computation of AAS is not affected by the discrepancy of recombination events across chromosomes and ethnicities, and we implemented the procedures as described in Barrie et al. (2024)[12] with SparsePainter.

We assumed the normality of LDAS for all ethnicities across the genome. We converted the LDAS into p-values through the normality test which aims to detect low LDAS, and we only focused on SNPs with p(LDAS) from at least one ethnic background that is significant at $p = 10^{-6}$. Those SNPs are classified as shared or ethnicity-specific low LDAS if p(LDAS) from all the other ethnic backgrounds are significant at $p = 0.05$, or insignificant at $p = 0.1$, respectively.

As AAS follows Gamma distribution and produces more extreme p-values, we employed a stricter significance level, $p = 10^{-50}$, for filtering SNPs with significant AAS. Similarly, those SNPs are categorized as having shared or ethnicity-specific significant AAS if p(AAS) from all the other ethnic backgrounds are significant at $p = 10^{-10}$, or insignificant at $p = 10^{-5}$, respectively.

Furthermore, to ensure robust results, we repainted UKB using 5 continental populations as delineated by the 1000GP continents (Europe, Africa, America, South Asia and East Asia) to obtain an alternate set of LDAS and AAS results. We then mapped each SNP with low LDAS and AAS signals to its gene (if the SNP overlaps with a gene) via R package 'gprofiler2', and visualised the results in Fig. 5 and Fig. 6.

Comparison of LDAS and AAS signals with natural selection in Bronze Age Britain and archaic adaptive introgression in 1000GP populations

Our LDAS and AAS analyses from painting 7 UK Biobank ethnic backgrounds with 1000GP populations have detected various signals of selection (Fig. 6 and Supplementary Tab. 1), and we investigated the overlaps with the other selection signals. By comparison with the genome-wide significant ($P < 10^{-7}$) selection signals in the ancient British data[43], we found the only overlap genes are HLA-DRB6 and HLA-DRB1 on chromosome 6. We compared loci that have been identified as exhibiting adaptive introgression from Neanderthal or Denisovan ancestries in the 1000GP populations[44]. Although none of them overlaps the genes with LDAS signals, we discovered that the ADARB2 gene, located on chromosome 10 overlaps with AAS signals. This gene experiences introgression from

Denisovan ancestry within the 1000GP PEL population, and coincides with the AAS signals in British, Irish, Indian, Caribbean and Chinese ethnicities. Notably, the utilization of different reference panels can probably lead to the identification of distinct genes exhibiting selection signals of LDAS and AAS.

Data availability

The phased 1000 Genomes Project data build GRCh37/hg19 are available at https://bochet.gcc.biostat.washington.edu/beagle/1000_Genomes_phase3_v5a/b37.vcf/. The UK Biobank data can be accessed by approved researchers through https://www.ukbiobank.ac.uk. We used the UK Biobank data under project 81499. The UK map data are available at https://gadm.org.

Code availability

The C++ code for SparsePainter is available on GitHub at https://github.com/YaolingYang/SparsePainter, and the website for SparsePainter is at https://sparsepainter.github.io/. PBWTpaint is available on GitHub at https://github.com/richarddurbin/pbwt.

Acknowledgements

We thank the participants in the UK Biobank (UKB) and 1000 Genomes Project (1000GP). Y.Y. was supported by China Scholarship Council [grant number 202108060092]. This work was carried out using the computational facilities of the Advanced Computing Research Centre, University of Bristol - http://www.bris.ac.uk/acrc.

Author contributions

Y.Y., R.D. and D.J.L. conceived and designed the project and methodology. D.J.L. supervised the project. Y.Y., R.D. and D.J.L. developed the methodology. R.D. and D.J.L. programmed the codes for PBWTpaint. Y.Y. programmed the codes for SparsePainter. Y.Y. did simulations and UKB data analysis under the supervision of D.J.L. A.K.N.I. analysed and interpreted genes with LDAS and AAS signals. Y.Y. wrote the initial manuscript draft. All authors wrote, reviewed, discussed and revised the subsequent versions of the manuscript (led by Y.Y. and D.J.L.). Y.Y. and A.K.N.I. wrote the Supplementary Information. All authors agreed with the submitted manuscript.

Competing interests

All authors have declared no competing interests.

References

1. Hellenthal, G. *et al.* A genetic atlas of human admixture history. *Science* **343**, 747–751 (2014).
2. Gravel, S. Population genetics models of local ancestry. *Genetics* **191**, 607–619 (2012).
3. Salter-Townshend, M. & Myers, S. Fine-scale inference of ancestry segments without prior knowledge of admixing groups. *Genetics* **212**, 869–889 (2019).
4. Green, R. E. *et al.* A draft sequence of the Neandertal genome. *Science* **328**, 710–722 (2010).
5. Bryc, K., Durand, E. Y., Macpherson, J. M., Reich, D. & Mountain, J. L. The genetic ancestry of African Americans, Latinos, and European Americans across the United States. *The American Journal of Human Genetics* **96**, 37–53 (2015).
6. Leslie, S. *et al.* The fine-scale genetic structure of the british population. *Nature* **519**, 309–314 (2015).
7. Price, A. L. *et al.* Sensitive detection of chromosomal segments of distinct ancestry in admixed populations. *PLoS Genetics* **5**, e1000519 (2009).
8. Zhang, J. & Stram, D. O. The role of local ancestry adjustment in association studies using admixed populations. *Genetic Epidemiology* **38**, 502–515 (2014).
9. Gouveia, M. *et al.* Unappreciated subcontinental admixture in Europeans and European Americans and implications for genetic epidemiology studies. *Nature Communications* **14**, 6802 (2023).
10. Peter, B. M. Admixture, population structure, and F-statistics. *Genetics* **202**, 1485–1501 (2016).
11. Buniello, A. *et al.* The NHGRI-EBI GWAS Catalog of published genome-wide association studies, targeted arrays and summary statistics 2019. *Nucleic Acids Research* **47**, D1005–D1012 (2019).
12. Barrie, W. *et al.* Elevated genetic risk for multiple sclerosis emerged in steppe pastoralist populations. *Nature* **625**, 321–328 (2024).
13. Schick, U. M. *et al.* Genome-wide association study of platelet count identifies ancestry-specific loci in Hispanic/Latino Americans. *The American Journal of Human Genetics* **98**, 229–242 (2016).
14. Hodonsky, C. J. *et al.* Ancestry-specific associations identified in genome-wide combined-phenotype study of red blood cell traits emphasize benefits of diversity in genomics. *BMC Genomics* **21**, 1–14 (2020).
15. Atkinson, E. G. *et al.* Tractor uses local ancestry to enable the inclusion of admixed individuals in GWAS and to boost power. *Nature Genetics* **53**, 195–204 (2021).
16. Wu, J., Liu, Y. & Zhao, Y. Systematic review on local ancestor inference from a mathematical and algorithmic perspective. *Frontiers in Genetics* **12**, 639877 (2021).
17. Li, N. & Stephens, M. Modeling linkage disequilibrium and identifying recombination hotspots using single-nucleotide polymorphism data. *Genetics* **165**, 2213–2233 (2003).
18. Lawson, D. J., Hellenthal, G., Myers, S. & Falush, D. Inference of population structure using dense haplotype data. *PLoS Genetics* **8**, e1002453 (2012).
19. Baran, Y. *et al.* Fast and accurate inference of local ancestry in Latino populations. *Bioinformatics* **28**, 1359–1367 (2012).
20. Browning, S. R., Waples, R. K. & Browning, B. L. Fast, accurate local ancestry inference with

FLARE. *The American Journal of Human Genetics* **110**, 326–335 (2023).

21. Brisbin, A. *et al.* PCAdmix: principal components-based assignment of ancestry along each chromosome in individuals with admixed ancestry from two or more populations. *Human Biology* **84**, 343 (2012).
22. Maples, B. K., Gravel, S., Kenny, E. E. & Bustamante, C. D. RFMix: a discriminative modeling approach for rapid and robust local-ancestry inference. *The American Journal of Human Genetics* **93**, 278–288 (2013).
23. Durbin, R. Efficient haplotype matching and storage using the positional Burrows–Wheeler transform (PBWT). *Bioinformatics* **30**, 1266–1272 (2014).
24. Sanaullah, A., Zhi, D. & Zhang, S. d-PBWT: dynamic positional Burrows–Wheeler transform. *Bioinformatics* **37**, 2390–2397 (2021).
25. Cormen, T. H., Leiserson, C. E., Rivest, R. L. & Stein, C. *Introduction to algorithms* (MIT press, 2022).
26. Consortium, . G. P. *et al.* A global reference for human genetic variation. *Nature* **526**, 68 (2015).
27. Pritchard, J. K., Stephens, M. & Donnelly, P. Inference of population structure using multilocus genotype data. *Genetics* **155**, 945–959 (2000).
28. Patterson, N., Price, A. L. & Reich, D. Population structure and eigenanalysis. *PLoS Genetics* **2**, e190 (2006).
29. McVean, G. A genealogical interpretation of principal components analysis. *PLoS Genetics* **5**, e1000686 (2009).
30. Hu, S. *et al.* Leveraging fine-scale population structure reveals conservation in genetic effect sizes between human populations across a range of human phenotypes. *bioRxiv* 2023–08 (2023).
31. Haller, B. C. & Messer, P. W. SLiM 3: forward genetic simulations beyond the Wright–Fisher model. *Molecular Biology and Evolution* **36**, 632–637 (2019).
32. Sarmanova, A., Morris, T. T. & Lawson, D. J. Population stratification in GWAS meta-analysis should be standardized to the best available reference datasets. *bioRxiv* (2020).
33. Bycroft, C. *et al.* The UK Biobank resource with deep phenotyping and genomic data. *Nature* **562**, 203–209 (2018).
34. Szpiech, Z. A. & Hernandez, R. D. selscan: an efficient multithreaded program to perform EHH-based scans for positive selection. *Molecular Biology and Evolution* **31**, 2824–2827 (2014).
35. Wysocki, T., Olesińska, M. & Paradowska-Gorycka, A. Current understanding of an emerging role of HLA-DRB1 gene in rheumatoid arthritis–from research to clinical practice. *Cells* **9**, 1127 (2020).
36. Kitaura, K., Shini, T., Matsutani, T. & Suzuki, R. A new high-throughput sequencing method for determining diversity and similarity of T cell receptor (TCR) α and β repertoires and identifying potential new invariant TCR α chains. *BMC Immunology* **17**, 1–16 (2016).
37. Howard-McCombe, J. *et al.* Genetic swamping of the critically endangered Scottish wildcat was recent and accelerated by disease. *Current Biology* **33**, 4761–4769 (2023).

38. Benton, M. L. *et al.* The influence of evolutionary history on human health and disease. *Nature Reviews Genetics* **22**, 269–283 (2021).
39. Holmes, E. C. & Twiddy, S. S. The origin, emergence and evolutionary genetics of dengue virus. *Infection, Genetics and Evolution* **3**, 19–28 (2003).
40. Messina, J. P. *et al.* Global spread of dengue virus types: mapping the 70 year history. *Trends in Microbiology* **22**, 138–146 (2014).
41. Browning, B. L., Tian, X., Zhou, Y. & Browning, S. R. Fast two-stage phasing of large-scale sequence data. *The American Journal of Human Genetics* **108**, 1880–1890 (2021).
42. Chen, T. & Guestrin, C. Xgboost: A scalable tree boosting system. In *Proceedings of the 22nd acm sigkdd international conference on knowledge discovery and data mining*, 785–794 (2016).
43. Mathieson, I. & Terhorst, J. Direct detection of natural selection in Bronze Age Britain. *Genome Research* **32**, 2057–2067 (2022).
44. Racimo, F., Marnetto, D. & Huerta-Sánchez, E. Signatures of archaic adaptive introgression in present-day human populations. *Molecular Biology and Evolution* **34**, 296–317 (2017).

Extended Data

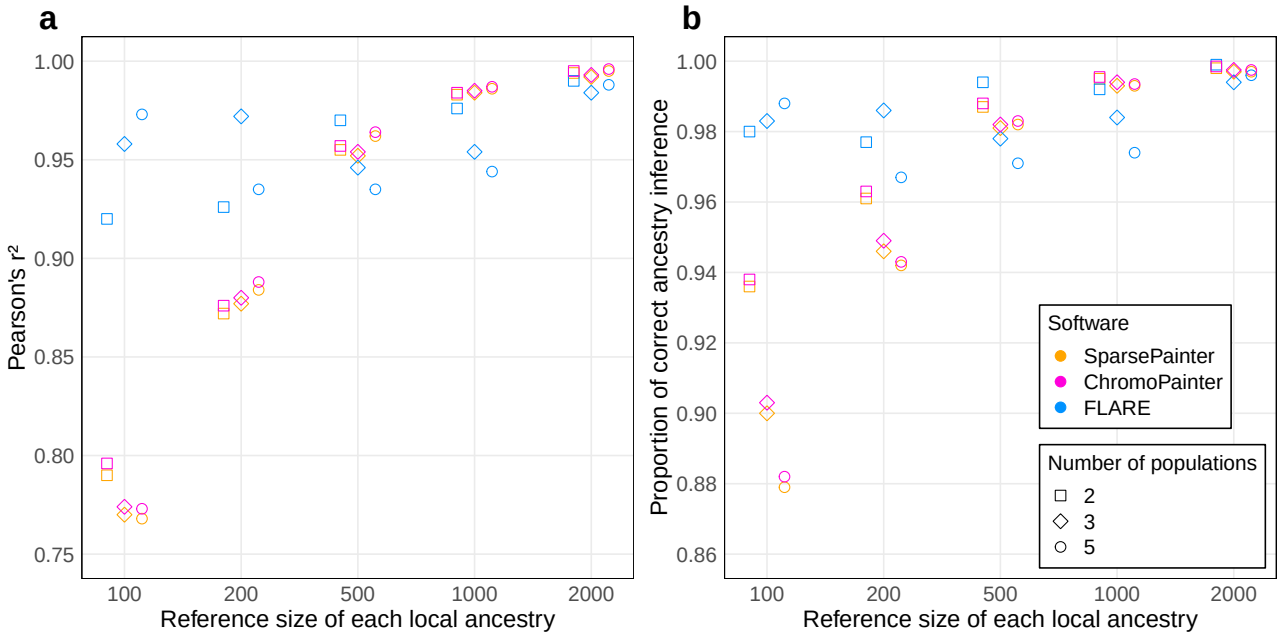

Extended Data Fig. 1: **Local ancestry estimation accuracy between software with different numbers of populations, reference sizes and earlier sampled target individuals.** This simulation has 3600 SNPs and 50 target individuals sampled 3 generations after admixture (Simulation 2b). The y-axis for the left and right plots are the squared Pearson's correlation coefficient and the proportion to correct ancestry inference, respectively, and the x-axis is the reference size of each reference ancestry.

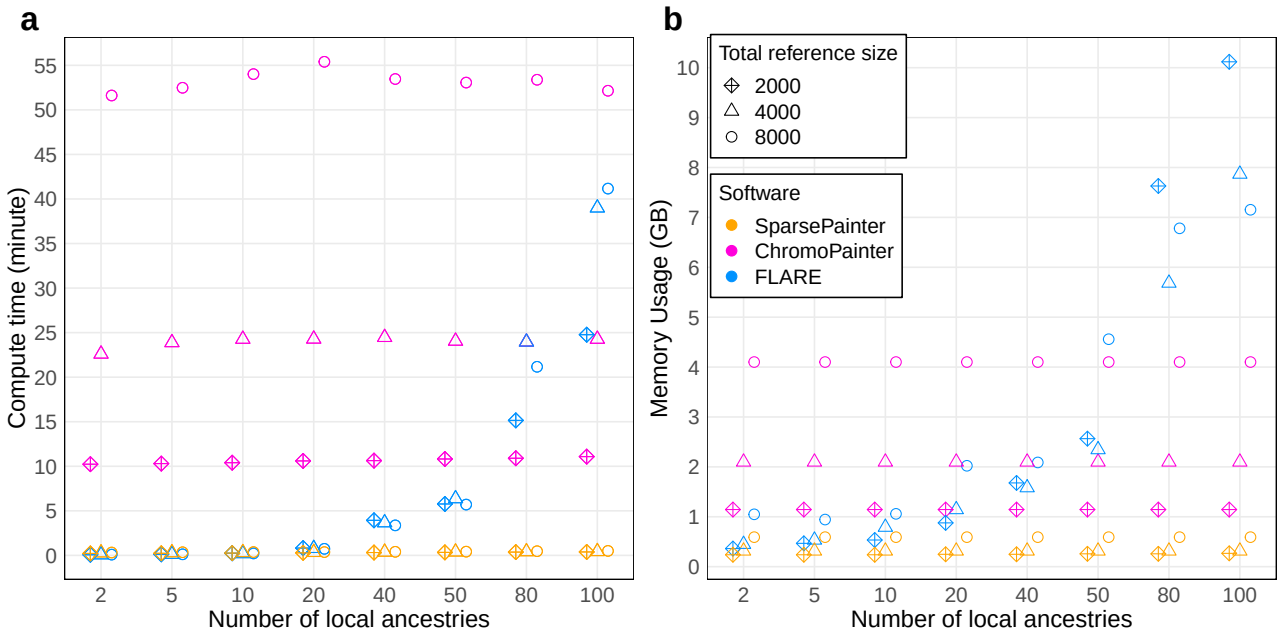

Extended Data Fig. 2: **Compute time and memory usage of painting 500 individuals between software with different numbers of local ancestries and reference sizes.** This simulation (Simulation 2a) has 2100 SNPs. The y-axis for the left and right plots are the compute time in minutes and the memory usage in GB, respectively, and the x-axis is the number of local ancestries.

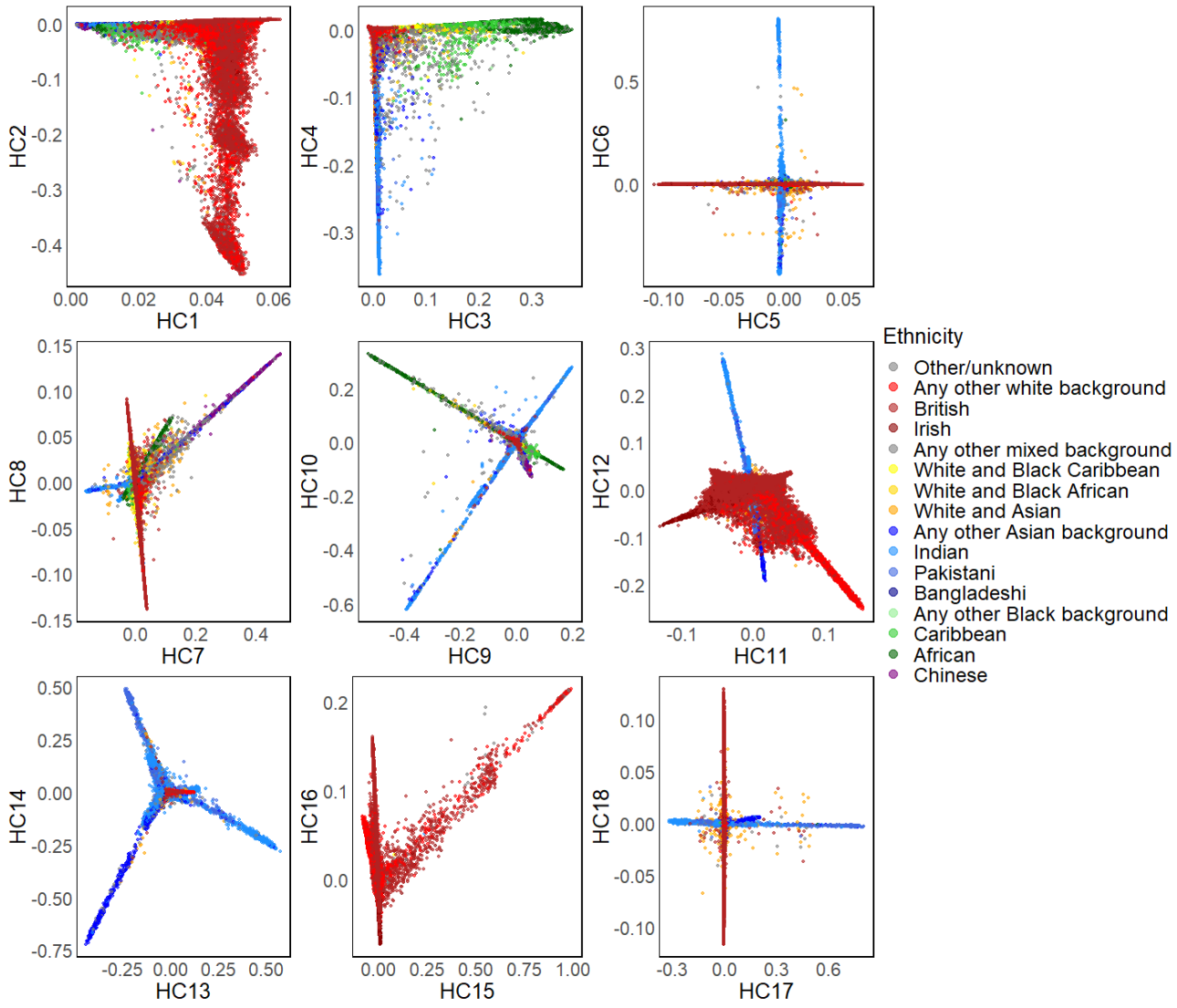

Extended Data Fig. 3: **Two-dimensional plots for the first 18 HCs stratified by UKB self-reported ethnic backgrounds (n=406,773 individuals).**

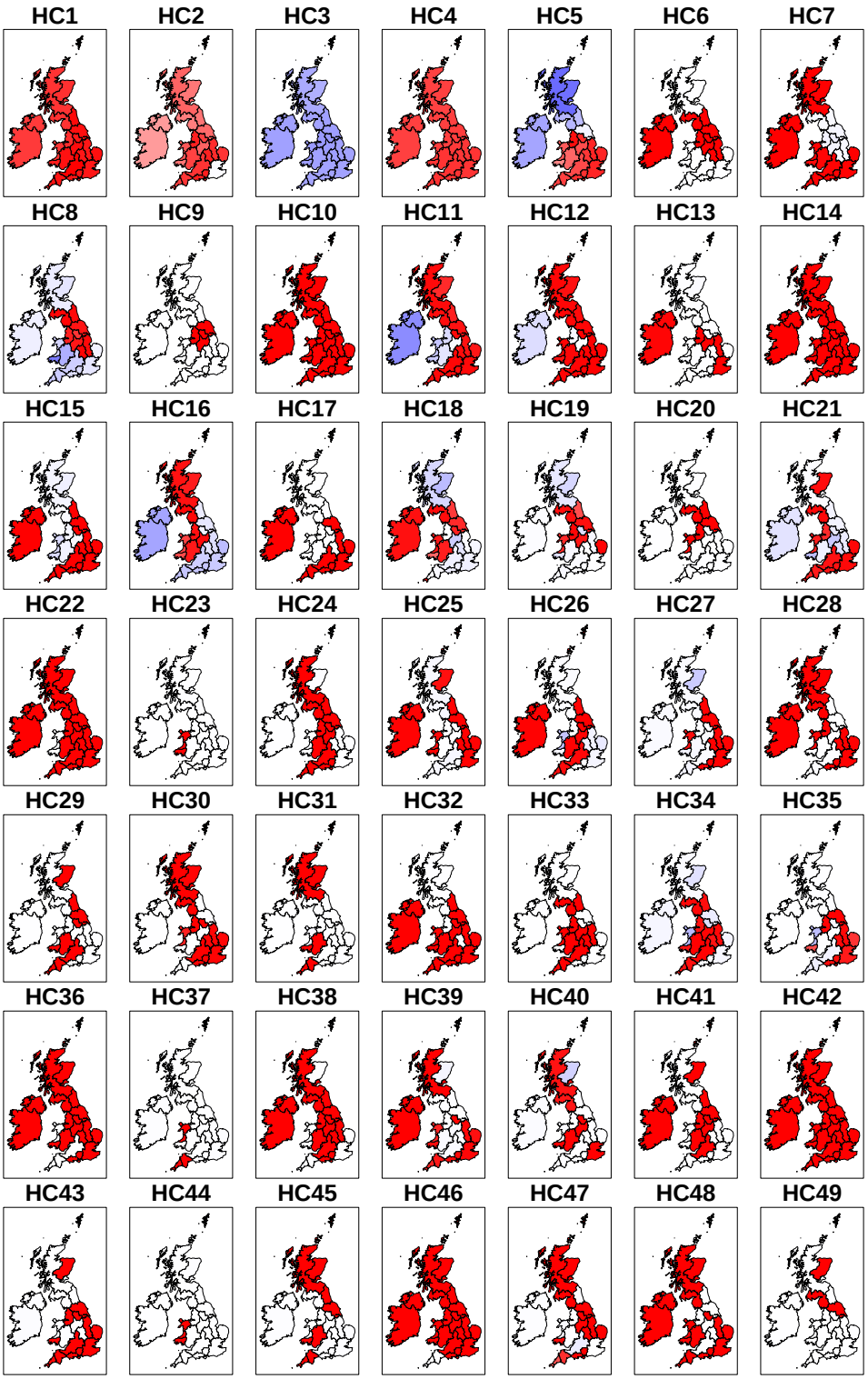

Extended Data Fig. 4: **Visualisation of the average of the first 49 HCs stratified by birthplaces within the UK and Ireland.** This analysis includes n=347,532 individuals. The average HC of each region bigger than, smaller than and equal to the worldwide average is coloured in red, blue and white, respectively.

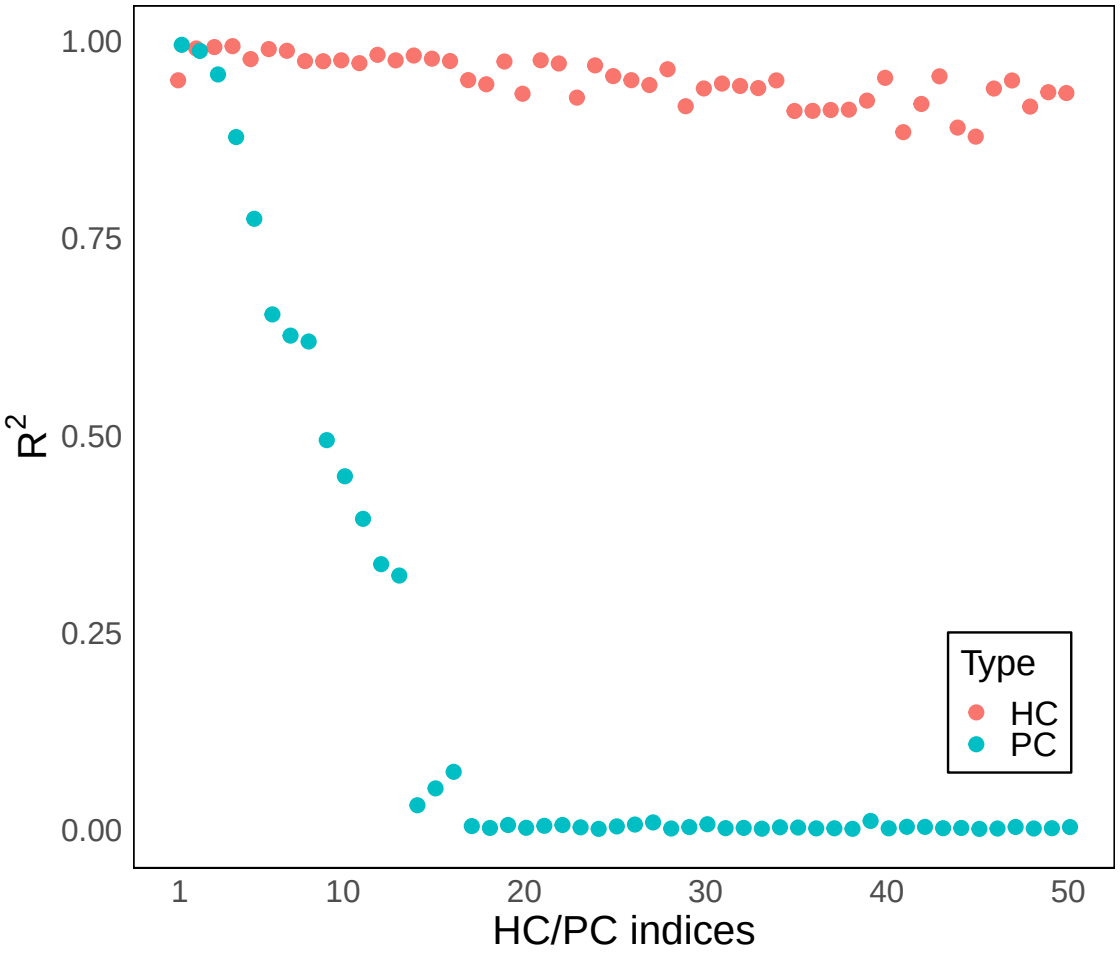

Extended Data Fig. 5: **Average Coefficient of determination for predicting top 50 HCs/PCs computed from odd (even) chromosomes using the first 150 HCs/PCs from even (odd) chromosomes of 406,773 individuals.** The top 50 HCs are well predicted from both plots, while only few top PCs can be predicted with high accuracy.

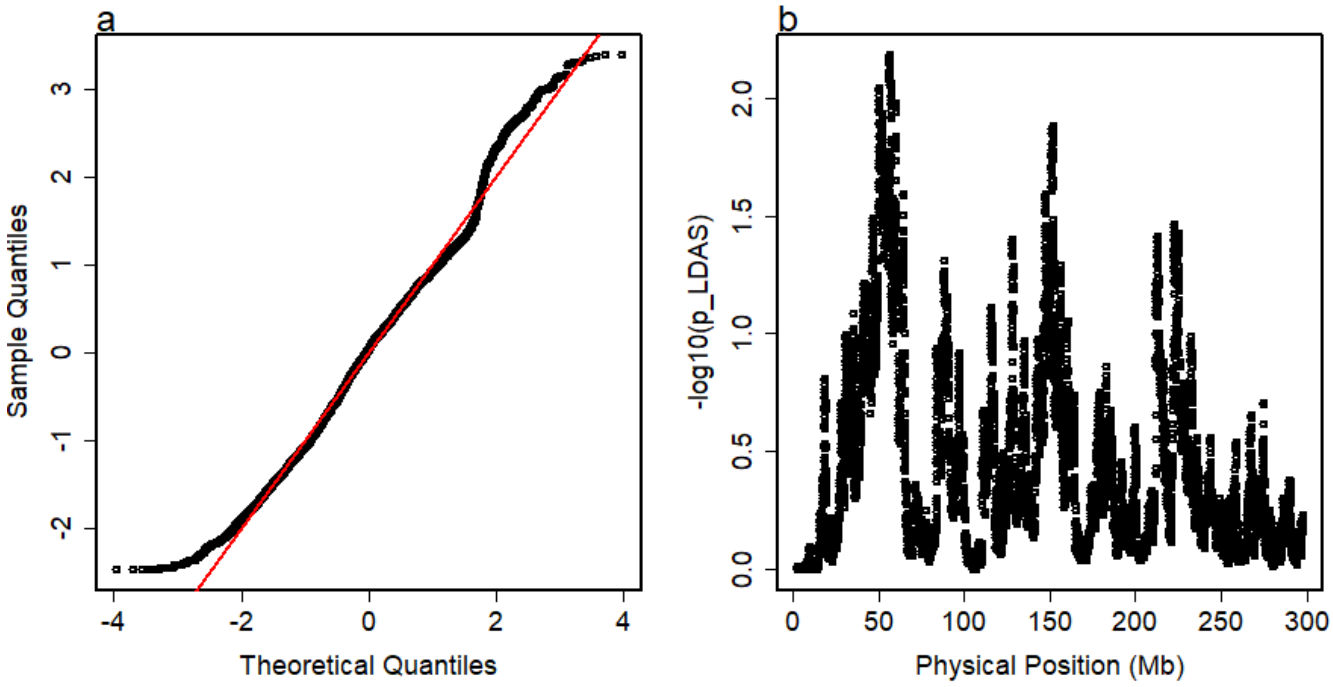

Extended Data Fig. 6: **Distribution of LDAS under the simulation of a 500Mb genome.** a, The quantile-quantile plot of the z-scores of LDAS. b, The P-values (represented in -log10 scale) under the normality test for detecting low LDAS across the simulated genome.

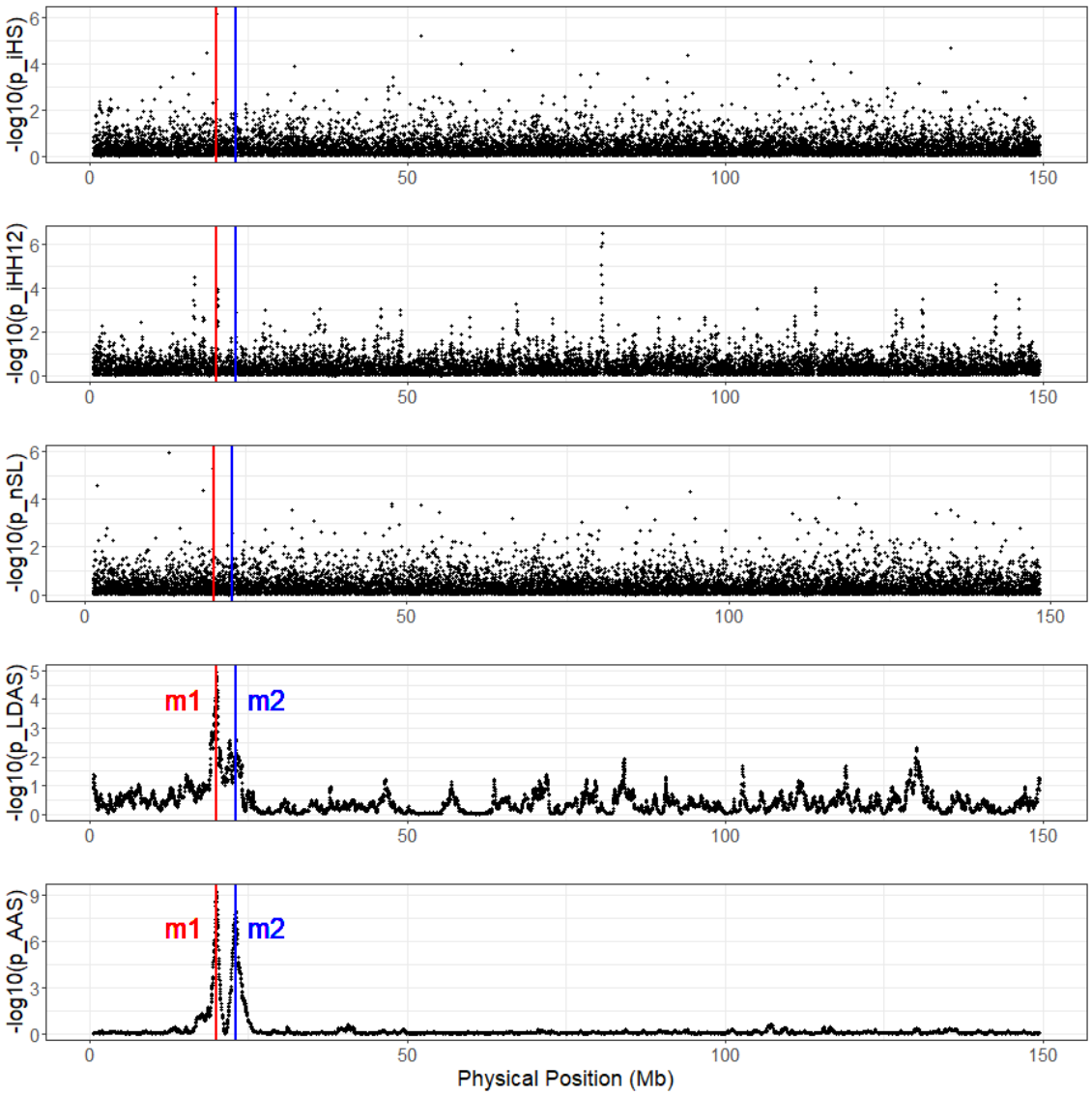

Extended Data Fig. 7: **iHS, iHH12, nSL, LDAS and AAS under two-loci positive position selection in both ancient and modern populations (reporting the -log10 of P-values).** The red and blue vertical lines indicate the loci under selection in population p1 and p2, respectively.

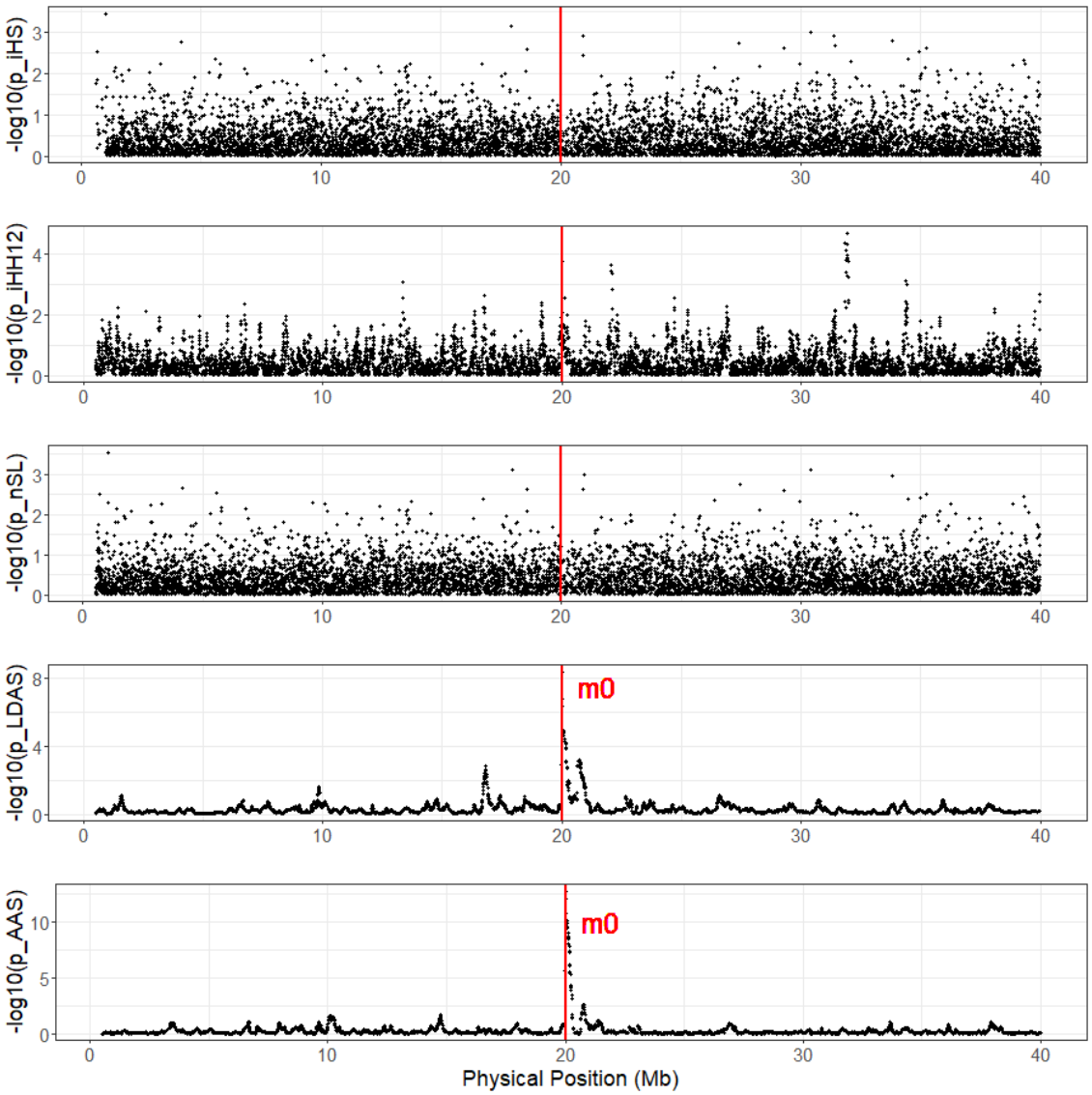

Extended Data Fig. 8: iHS, iHH12, nSL, LDAS and AAS under one-locus positive selection in ancient populations and negative selection in modern population (reporting the -log10 of P-values). The red vertical line indicates the loci under selection.

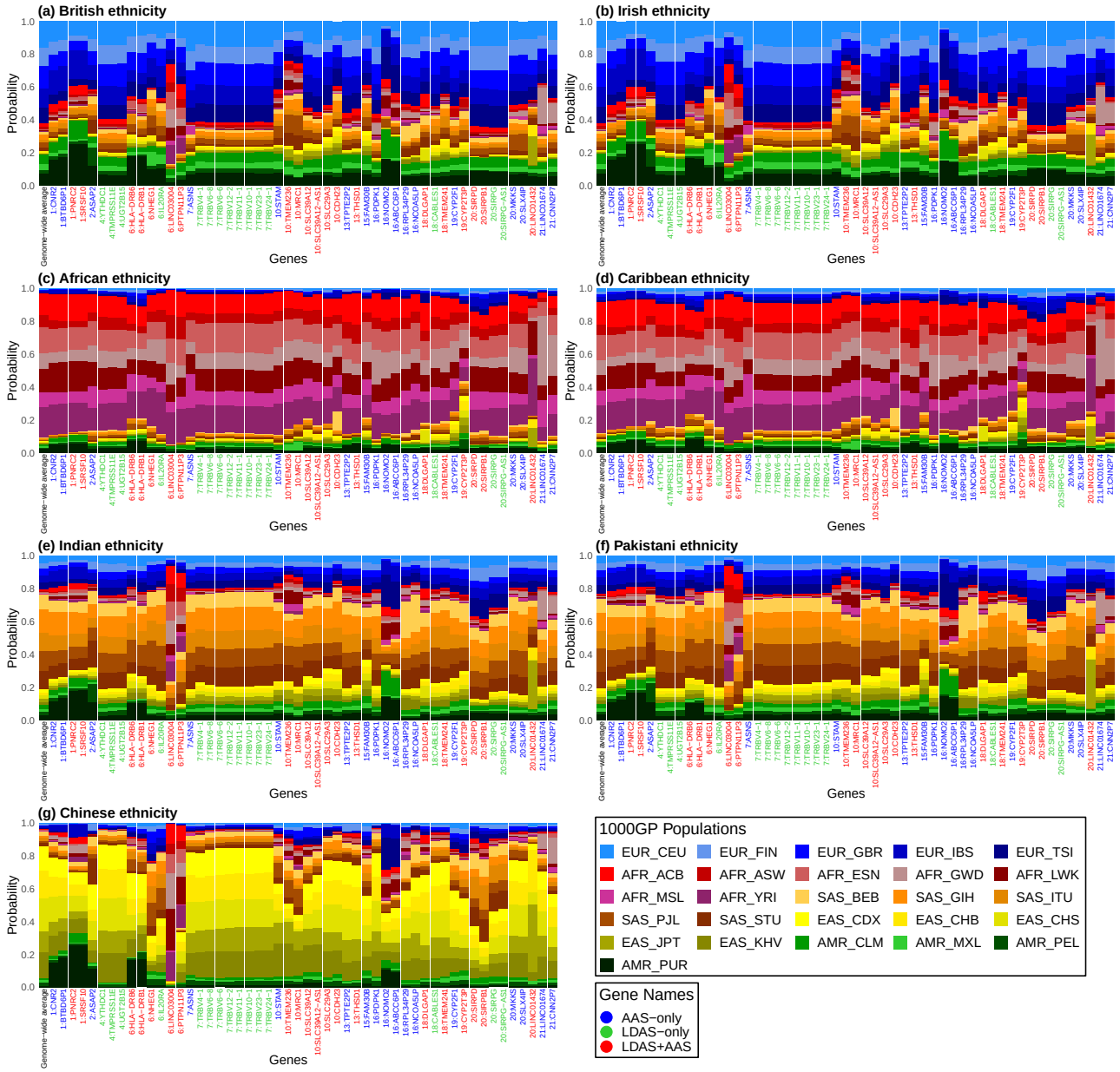

Extended Data Fig. 9: **Average probabilities of 26 1000GP populations at genes with shared LDAS and AAS signals across 7 UK Biobank self-reported ethnicities.** We sampled a representative SNP from each gene with low LDAS or AAS signals (in 26-pop painting) shared between all 7 UKB ethnicities, as visualised in Fig. 6. The genome-wide average probabilities are shown on the left of each plot for comparison.